Cost-based comparison between membrane systems and chemical absorption processes for CO_2 capture from flue gas

Ana M. Arias[1], Patricia L. Mores[1], Nicolás J. Scenna[1], José A. Caballero[2], Miguel C. Mussati[3], Sergio F. Mussati[3,*]

[1] CAIMI Centro de Aplicaciones Informáticas y Modelado en Ingeniería, Universidad Tecnológica Nacional, Facultad Regional Rosario, Zeballos 1346, S2000BQA Rosario, Argentina.

[2] Department of Chemical Engineering, University of Alicante, Apartado de correos 99, 03080 Alicante, Spain.

[3] INGAR Instituto de Desarrollo y Diseño (CONICET-UTN), Avellaneda 3657, S3002GJC Santa Fe, Argentina.

[*] Corresponding author: mussati@santafe-conicet.gov.ar

Abstract

In this paper, a cost comparison between two-stage membrane-based systems and amine-based chemical absorption processes for post-combustion CO_2 capture from flue gas is performed for the same design specifications. The comparison is based on the optimal solutions obtained by minimization of the total annual cost while meeting a target CO_2 recovery level of 90% and a CO_2 purity level of at least 0.95 mole fraction. A wide range of CO_2 concentration values in the feed stream was considered, from 0.04 to 0.44 CO_2 mole fraction, which is representative of several CO_2-generating processes (natural gas and coal-fired power plants, refinery processes, and cement and steel production plants, among other industries). To this end, nonlinear mathematical programming problems formulated for both processes were solved using gradient-based optimization algorithms, which allow the simultaneous optimization of the process configuration, sizes of the pieces of equipment, and operating conditions.

Based on the considered cost model, the chemical absorption process resulted to be the preferred technology −in terms of the total annual cost− over the membrane system when treating diluted flue gases, with feed CO_2 mole fractions up to about 0.23; conversely, the membrane-based system becomes the cheapest technology for CO_2 mole fractions higher than 0.24. For instance, for 0.16 mole fraction of CO_2, the optimal total annual cost obtained for the amine-based process is 23.24% lower than that for the membrane-based system; but for 0.41 mole fraction of CO_2, the optimal total annual cost obtained for the membrane system is 30.75% lower than that for the chemical absorption process.

Based on this, the proposed optimization models constitute a valuable decision-support tool for designing, simulating, and optimizing amine-based chemical absorption processes and membrane-based systems for post-combustion CO_2 capture, and the obtained results can serve as a

guide to assist in selecting the best between both technologies, in terms of cost, for a particular industrial case.

Keywords: Greenhouse gas emissions; CO_2 capture; Membrane; Chemical absorption; Amines; Optimization; NLP; GAMS.

I. Introduction

Carbon dioxide (CO_2) capture and storage (CCS) and CO_2 capture and utilization (CCU) are the most important strategies to reduce the global CO_2 emissions. They differ in the final destination of the captured CO_2. In CCS, the captured CO_2 is transported to suitable burial sites. In CCU, the captured CO_2 is utilized to produce value-added products. Recent advances in CCS and CCU can be found in Cuéllar-Franca and Azapagic [1] and Kravanja et al. [2].

Carbon dioxide capture by means of amines is the most mature technology available today. Since it can be assembled at the end-of-the-pipe of existing power plants, it is appropriate to retrofit them without requiring significant modifications [3]. However, this technology requires high energy consumption for amine regeneration [4,5]. For this reason, a considerable research effort has been dedicated to minimizing the energy requirement. In this sense, some of the research activities are: a) the optimization employing advanced computational tools considering the entire process [6], b) the development of novel solvents at laboratory scale [7,8] and also by using computer-aided molecular design (CAMD) [9−14], and c) the evaluation of several solvents in pilot plants [15−17]. In addition, the amine loss and degradation, and the unavoidable equipment corrosion are also weaknesses of this technology [18−20].

Membrane-based processes for post-combustion CO_2 capture have been studied by several researchers [21−29]. Unlike the amine-based systems, no steam is required to operate the separation process and no environmental impact is caused by amine loss and degradation. However, with the current state of membrane development, high CO_2 capture levels and product purity values cannot be simultaneously attained using a single-stage membrane configuration [24,30]. This limitation can be overcome by means of multi-stage membrane configurations [22,24,29,30]. Despite the electric power required for permeate recompression, Arias et al. [22], He et al. [24], and Zhai and Rubin [29] showed that the multi-stage membrane configurations compete with the amine-based post-combustion capture processes −in terms of energy consumption− to obtain same target levels of CO_2 recovery and purity. This comparison is based on the equivalent power of the steam used for the

amine regeneration in the absorption-based capture process and the electric power required by the membrane-based capture process. The importance to optimize multi-stage membrane configurations by using a cost-based approach and to consider all the trade-offs among the process variables at the design stage has been highlighted by Arias et al. [22] and Lindqvist et al. [30].

This paper is a follow-up of the works previously presented by Arias et al. [22] and Mores et al. [31]. It proposes the application of the mathematical programming and simultaneous optimization approaches presented in Arias et al. [22] for multi-stage membrane systems and in Mores et al. [31] for amine-based chemical absorption processes to compare the optimal solutions obtained for both processes for the same design specifications. A wide range of CO_2 concentration values in the feed stream is investigated, which is representative of several CO_2-generating processes such as natural gas and coal-fired power plants, refinery processes, and cement and steel production plants.

The paper is outlined as follows. Section 2 describes the examined processes. Section 3 summarizes the main assumptions, considerations, and equations of the process mathematical models. Section 4 states the optimization problems to be solved. Section 5 presents and discusses the obtained results. Finally, Section 6 points out the conclusions of the investigation and future works.

2. Process description

2.1. Membrane-based systems for post-combustion CO_2 capture

Pressure-driven membrane processes operate on the principle of selective permeation, where components with higher permeation rates pass through the membrane module faster than components with lower permeation rates. The driving force for permeation is the partial pressure difference of the gas components between the feed and permeate sides, which can be generated in different ways: a) compression of the feed stream, b) application of vacuum on the permeate side, and c) application of a sweep gas on the permeate side. Due to the low pressure and CO_2 concentration of power plant flue gases, the driving force is too low for membrane processes for post-combustion CO_2 capture. Compression is usually preferred because the capital cost of vacuum piece of equipment is twice −or even more− higher than that of compression piece of equipment of the same power rating [26], but needs higher power consumption [32].

Membrane processes show increased separation performances with increasing CO_2 concentration in the feed mixture [33−35].

The energy required for recovering CO_2 by means of membrane processes depends on several factors such as the target purity level, flue gas composition, and membrane selectivity for CO_2. Even

though they are considered as energy-saving processes compared to the chemical absorption processes, they can require high energy consumptions for CO_2 capture from feed streams with low CO_2 partial pressures, especially when high levels of both recovery and purity are desired.

Membrane-based processes are simple and easy to operate. There are no moving parts (except for pumps and compressors) and, therefore, no complex control schemes are required.

Figure 1 shows a schematic of the studied two-stage membrane system. The incoming gas stream F is directed to the feed compressor COM1 to increase the pressure and, afterward, it is directed to the membrane stage MEM1 which generates two streams: a CO_2-lean retentate stream R1 and a CO_2-enriched permeate stream P1. Vacuum is usually applied at the permeate side through the vacuum pump PUMP1 to increase the driving force for the permeation process. The retentate stream is passed through the expander EXP to recovery mechanical power and it is emitted to the environment afterward. The permeate stream obtained in MEM1 increases its pressure by passing through the compressor COM2 and it is fed to the second membrane stage MEM2. The resulting retentate stream is recycled back to MEM1 and it is mixed with the incoming feed. While the permeate stream is compressed in COMP to the conditions required for transportation.

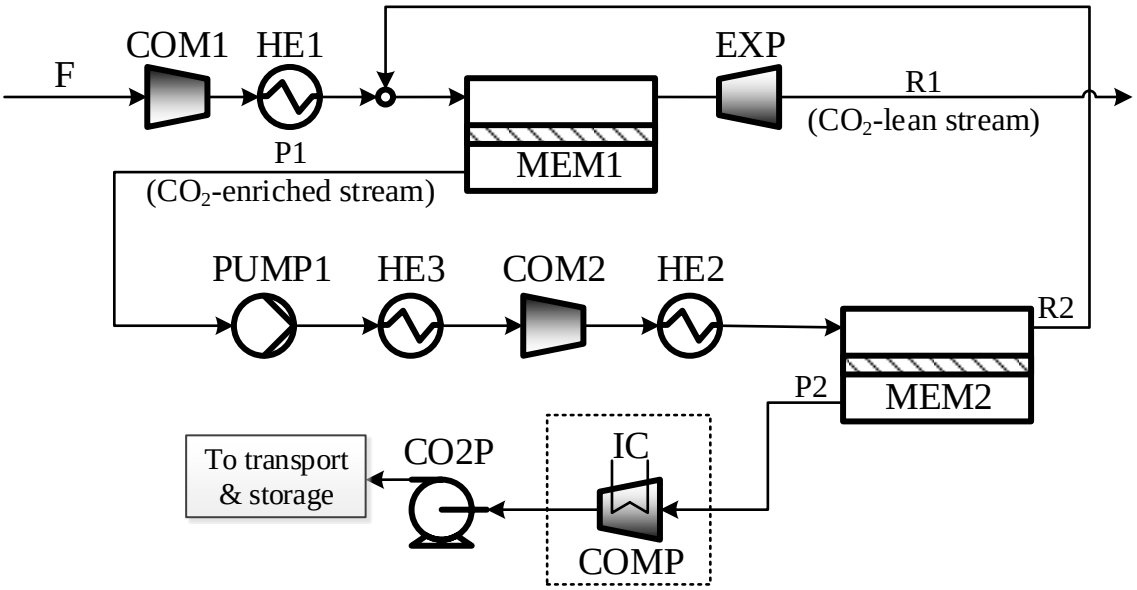

Figure 1. Schematic of a two-stage membrane system for post-combustion CO_2 capture.

Multi-stage membrane systems are superior than single-stage ones to achieve both high recovery and product purity levels but require greater membrane area and higher power for compression. Indeed, there are several trade-offs among the CO_2 recovery and purity, membrane area, and power required by the compressor and/or vacuum pump −depending on how the CO_2

partial pressure difference across the membrane is created− that have to be elucidated at the process synthesis and design stages. The lower the pressure difference, the lower the power requirement but the higher the membrane area. The number of trade-offs increases with the number of stages since more relationships are established among the process variables.

2.2. Amine-based chemical absorption processes for post-combustion CO_2 capture

Figure 2 shows a schematic of the conventional chemical absorption process for post-combustion CO_2 capture using amines as solvent. It consists of three major sections: absorption, amine regeneration, and CO_2 final compression. The main process units are the absorption column ABS and the regeneration column REG with a steam reboiler REB and a condenser COND. Packed columns are usually used in order to improve the interphase contact requiring the inclusion of additional pieces of equipment. A blower BLOW is required to propel the feed gas stream to the absorber ABS and a pump RAP is required to move the liquid stream to the regenerator REG. The CO_2 lean-rich amine solution heat exchanger AAHE and the CO_2 lean amine-water cooler AWHE are included for energy integration. The flue gas is fed at the bottom of the absorber ABS and the lean amine solution is fed at the absorber top. The CO_2 content in the gas stream is chemically absorbed by the amine forming a carbamate ion ($MEACOO^-$). The amine is regenerated in the REG and sent back to the ABS. The cleaned flue gas is emitted to the environment from the absorber top. The CO_2-enriched amine solution leaving the absorber bottom is pumped by RAP through the solution heat exchanger AAHE −where is preheated with the CO_2-lean amine solution leaving the REG– to the top of the regeneration column REG. The CO_2-lean amine solution is directed from the steam reboiler REB of the REG to the top of the ABS through the heat exchanger AAHE and the cooler AWHE for further CO_2 removal. While the gas mixture of steam, MEA, and CO_2 is directed to the condenser COND for recovering and recycling H_2O and MEA. Finally, the obtained CO_2-enriched stream leaving the COND is conveyed to successive stages of compression and inter-cooling to achieve a pressure of 13.8 MPa for pipe transportation.

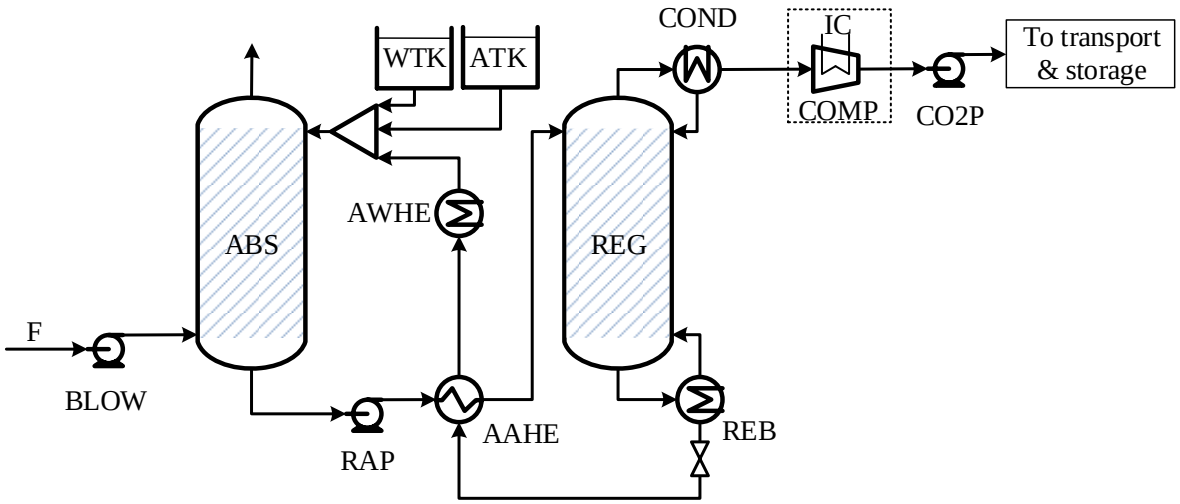

Figure 2. Schematic of a conventional amine-based chemical absorption process for post-combustion CO_2 capture.

There are many strong trade-offs among the type of the used solvent, steam temperature and pressure, target CO_2 removal level, sizes of the pieces of equipment (heat exchangers, reboiler, condenser, absorber, regenerator, pumps, and compressors), and operating conditions (flow rates, pressures, and temperatures) that affect the overall efficiency and cost of the absorption-desorption process. For instance, the solvent type and flow rate influence both the ABS and REG. For instance, the higher the solvent concentration, the higher the CO_2 absorption capacity in the ABS with lower flow rates and heat duties in the REG. However, the higher the solvent concentration, the higher the risk of corrosion problems requiring materials more resistant in the ABS and REG and, consequently, higher investments. Then, it is clear that the simultaneous optimization of the process variables is essential to determine the best design of the amine-based CO_2 capture process.

3. Process modeling

3.1. Membrane-based CO_2 capture process

3.1.1. Main model assumptions and considerations

The main assumptions made to formulate the mathematical model of a membrane unit are as follows [22]:

− All components are able to permeate through the membrane.

− The component permeability in the mixture is the same as the pure gas. The permeability does not depend on the operating pressure.

− Negligible pressure drops of the feed and permeate streams are assumed along the flow path.

− The high operating pressure value is the same for all the membrane stages.
− Plug flow pattern is assumed at both membrane sides.
− Isothermal conditions are considered for all membrane stages.
− Component mass transfer rate is modeled by the Fick's first law.

3.1.2. Mathematical model

The main constraints of the mathematical model used in this work to describe a generic membrane stage are presented in Appendix A and the complete mathematical model is provided as Supplementary Material to this article.

3.2. Amine-based CO_2 capture process

3.2.1. Main model assumptions and considerations

The main assumptions made to formulate the mathematical model of an absorption-regeneration train are as follows [36−39]:

− The reaction system is modeled by reactions r1 to r7. The first five reactions are equilibrium reactions while the last two are considered as pseudo-first-order reactions to take into account the reaction effect on the mass transfer through the enhancement factor.

$$2H_2O \leftrightarrow H_3O^+ + OH^- \quad \text{r1}$$

$$2H_2O + CO_2 \leftrightarrow H_3O^+ + HCO_3^- \quad \text{r2}$$

$$H_2O + HCO_3^- \leftrightarrow H_3O^+ + CO_3^{2-} \quad \text{r3}$$

$$H_2O + MEAH^+ \leftrightarrow H_3O^+ + MEA \quad \text{r4}$$

$$MEACOO^- + H_2O \leftrightarrow MEA + HCO_3^- \quad \text{r5}$$

$$MEA + CO_2 + H_2O \leftrightarrow MEACOO^- + H_3O^+ \quad \text{r6}$$

$$CO_2 + OH^- \leftrightarrow HCO_3^- \quad \text{r7}$$

− Packed columns are used to carry out the CO_2 absorption and amine regeneration processes. They are modeled as a series of non-equilibrium stages with chemical reactions.
− The height of the columns is calculated by the number of transfer units (NTU) and the height of a transfer unit (HTU).
− The two-film resistance theory is used to describe the mass transfer phenomena.
− Reboiler and condenser are modeled as equilibrium stages.
− The solubility of CO_2 in MEA solutions is estimated using the Kent-Eisenberg model and the fugacity coefficients are estimated using the Peng-Robinson EOS for multi-component mixtures.

198 − A maximum temperature of 393 K is allowed in the reboiler to prevent amine degradation and
199 equipment corrosion [40−43].
200 − Dependence of thermodynamic and physico-chemical properties (solubility, density, viscosity,
201 diffusivity, fugacity, and enthalpy) with temperature and composition, pressure drop in the
202 absorption and regeneration columns, and mass transfer coefficients are calculated by the
203 correlations collected by Mores et al. [36,37].
204 − A centrifugal compressor with five intercooling stages is used for CO_2 compression. The CO_2-
205 enriched stream is compressed from the pressure at the regenerator top −which is an optimization
206 variable because it depends on the pressure drop in the regenerator− to 7.38 MPa. Then, the CO_2-
207 enriched stream is pumped up to 13.8 MPa for transportation.
208 − Water that is removed in the cooling process is sent back to the capture plant.
209 − The global heat transfer coefficients of the heat exchangers are assumed to be constant values.
210
211 **3.2.2. Mathematical model**
212 The main constraints of the mathematical model used in this work to describe a generic
213 absorption-desorption train are presented in Appendix B and the complete mathematical model is
214 provided as Supplementary Material to this article.
215
216 **4. Process optimization**
217 **4.1. Problem statement**
218 The optimization work consists in obtaining the optimal configuration, operating conditions,
219 and process unit sizes of the studied two-stage membrane system and amine-based chemical
220 absorption process for post-combustion CO_2 capture that minimize the total annual cost to treat a flue
221 gas stream with a flow rate of 22.32 kmol/s and CO_2 concentration values ranging between 0.04 and
222 0.44 mole fraction, while satisfying a fixed CO_2 recovery level of 90 % and a CO_2 purity level of at
223 least 0.95 mole fraction.
224
225 **4.2. Mathematical optimization model**
226 Formally, the nonlinear mathematical programming (NLP) optimization problem to be solved
227 for each process can be formulated as follows:

Minimize TAC

s.t.:

$$\begin{cases} \mathbf{h}_s(\mathbf{x}) = \mathbf{0}, \forall s \\ \mathbf{g}_t(\mathbf{x}) \le \mathbf{0}, \forall t \\ F = 22.32 \text{ kmol/s} \\ x_{F,CO_2} = p, \ 0.04 \le p \le 0.44 \\ R_{CO_2} = 90\% \\ x_{P,CO_2} \ge 0.95 \end{cases} \quad (1)$$

where TAC is the total annual cost −objective function to be minimized− which considers both operating and investment costs; **x** is the optimization variable vector (see Table 1); $\mathbf{h}_s(\mathbf{x})$ refers to equality constraints (mass, energy, and momentum balances; correlations to estimate physico-chemical properties; and expressions for process unit design); and $\mathbf{g}_t(\mathbf{x})$ refers to inequality constraints, which are used, for instance, to avoid temperature cross situations, and to impose lower and upper bounds on some critical operating variables. F refers to the total feed flow rate, and $x_{F,CO2}$ is the CO_2 concentration in the feed stream which is assigned parametrically a fixed value p in each optimization run. R_{CO2} is the target CO_2 recovery level, and $x_{P,CO2}$ is the target CO_2 purity level i.e. the CO_2 concentration in the product stream.

Table 1. Optimization variables

Amine-based CO_2 capture	Membrane-based CO_2 capture
− Pressure, composition, and temperature profiles along the absorber and regenerator units.	− Compression pressure in the stages.
− Amine and cooling water flow rates.	− Permeate and retentate flow rates in the stages.
− Sizes of process units: 1) heat transfer area of the condenser, reboiler, MEA cooler, economizer, and inter-stage coolers, 2) packing volume of the absorber and regenerator (both height and diameter).	− Sizes of the process units: heat transfer area of heat exchangers and membrane area in the stages.
− Heat loads in the reboiler, condenser, and heat exchangers (amine-amine and amine-cooling water).	− Heat loads in the heat exchangers involved in the stages.
− Electric power required by pumps, blowers, and compressors.	− Electric power demanded by compressors and electric power generated by the expander.

The total annual cost TAC −expressed in M$/yr.− is calculated using Eq. (2), which includes the capital expenditures (CAPEX) annualized by a capital recovery factor (CRF) and the annual operating expenditures (OPEX):

$$TAC = CRF \cdot CAPEX + OPEX \quad (2)$$

The CAPEX includes the total direct manufacturing cost (DMC), the total indirect manufacturing cost (IMC), working investment (WI), and the start-up cost. Each cost item is calculated in terms of the total equipment acquisition cost (C_{inv}) using economic indexes (Table 2) which are assumed according to the guidelines given by Abu-Zahra et al. [44] and Rao and Rubin [45]. As indicated in Eq. (3), CAPEX results to be approximately five times (f_1 = 4.99) the total equipment acquisition cost.

$$CAPEX = f_1 \cdot C_{inv} \quad (3)$$

The capital recovery factor is calculated by Eq. (4) in terms of the interest rate (i) and the project lifespan (n):

$$CRF = \frac{i(1+i)^n}{(1+i)^n - 1} \quad (4)$$

Table 2. Capital expenditures (CAPEX)

Capital expenditures, CAPEX	**CAPEX = 1.35·IFC = 4.99·C_{inv}**
Invest. in fixed capital, IFC	1.0·IFC (=DMC+IMC)
Working investment, WI	0.25·IFC
Start-up cost	0.10·IFC
Direct manufacturing costs, DMC	*DMC = 2.688·C_{inv}*
Equipment acquisition cost, C_{inv}	1.0·C_{inv}
Equipment installation	0.528·C_{inv}
Piping	0.4·C_{inv}
Instrumentation and control	0.2·C_{inv}
Services facilities	0.2·C_{inv}
Electrical	0.11·C_{inv}
Building and services	0.1·C_{inv}
Yard improvements	0.1·C_{inv}
Land	0.05·C_{inv}
Indirect manufacturing costs, IMC	*IMC=0.375·DMC = 0.375·2.688·C_{inv}*
Contingencies	0.17·DMC
Engineering	0.1·DMC
Construction expenses	0.1·DMC
Contractor's fee	0.005·DMC

The total equipment acquisition cost is calculated by Eq. (5) as the sum of the acquisition costs (C_{inv}^k) of the individual pieces of equipment (k) which depend on their sizes (X^k) and constructive characteristics, as expressed by Eq. (6):

$$C_{inv} = \sum_k C_{inv}^k \quad (5)$$

$$C_{inv}^{k} = C_{0}^{k}\left(\frac{X^{k}}{X_{0}^{k}}\right)^{0.6} \quad (6)$$

Table 3 lists the numerical values of the reference costs of the pieces of equipment considered to calculate the total capital investment. They were updated considering the 2014 CEPCI indexes [46]. In order to obtain a consistent costing model, the equipment reference cost C_0^k and reference capacity X_0^k were adopted from Seider et al. [47], except for the reference costs of the membrane, membrane frame, and CO_2 pump. The membrane and frame costs are taken from Roussanaly et al. [27] and the CO_2 pump cost from McCollum and Ogden [28].

Table 3. Reference costs C_0^k used to calculate the equipment investment

Equipment	Ref. cost (M$)	Ref. capacity		Characteristics
Vessel (ABS, REG)	1.07013	80079	Kg	Vertical, SS
Packaging(ABS,REG)	0.98808	1000	m^3	Intalox saddles, ceramic, nominal diameter 0.05 m
Pump (PUMP)	0.00882	0.2217	m^3s^{-1} $m^{0.5}$	Centrifugal, SS (H=15.24 m; Q=0.0568 m^3/s)
Pump motor	0.00671	75	kW	Electrical, 3600 rpm, open Shell
Blower (BLOW)	0.26917	750	kW	Centrifugal, electric motor
Heat exchanger (AAHE)	0.45417	929	m^2	Floating head, SS-SS
Heat exchanger (AWHE, COND, IC)	0.35736	929	m^2	Floating head, CS-SS
Reboiler (REB)	0.61307	929	m^2	Kettle, SS-SS
Tanks (WTK, ATK)	0.63075	4500	m^3	Floating roof
Membrane (MEM)	0.05234	1000	m^2	Polymeric
Membrane frame (MEM)	0.238	2000	m^2	–
Compressors (COM) / Expander (EXP)	2.79	2000	kW	Centrifugal, electric motor, SS
CO_2 pump (CO_2P)	6.53	5000	kW	Centrifugal, electric motor

The annual operating expenditures (OPEX) are calculated using Eq. (7):

$$OPEX = PC + AC \quad (7)$$

where PC and AC refer to the production and additional costs, respectively, which can be calculated in terms of the cost of reposition materials and utilities (C_{rm}), manpower (C_{mp}), and other costs related to the total investment cost (C_{inv}), as given by Eq. (8):

$$OPEX = f_2 C_{rm} + f_3 C_{mp} + f_4 C_{inv} \quad (8)$$

The economic indexes f_2 (1.0550), f_3 (2.4499), and f_4 (0.4648) can be estimated from Table 2 and Table 4, which are based on the guidelines given by Abu-Zahra et al. [44] and Rao and Rubin [45].

The cost of raw materials and utilities C_{rm} is calculated using Eq. (9), which is a function of the annual consumption (m^u) and the specific cost (C_{rm}^u). Specifically, Eq. (9) considers the consumption of electricity, low-pressure steam, cooling water, MEA make up, and membrane reposition; their associated specific costs are listed in Table 5. A nominal loss of 1.5 kg of MEA per tonne of CO_2 is assumed [45,49]. In addition, an extra 20 % of the cost of the nominal MEA loss is considered for the corrosion inhibitor cost [45]. The annual membrane replacement rate is assumed to be 20 % [29].

$$C_{rm} = \sum_u C_{rm}^u \, m^u \quad (9)$$

Table 4. Operating and maintenance expenditures (OPEX)

Operative expenditures, OPEX = PC+AC = $f_2 \cdot C_{rm} + f_3 \cdot C_{mp} + f_4 \cdot C_{inv}$	
Total production costs, PC=FC+DPC+POC	
− Fixed charges, FC=(1)+(2)	
(1) Local taxes	$0.02 \cdot IFC$
(2) Insurance	$0.01 \cdot IFC$
− Direct production costs, DPC=(3)+(4)+(5)+(6)+(7)+(8)	
(3) Reposition material and utilities (C_{rm})	$1.0 \cdot C_{rm}$
(4) Operative manpower (C_{mp})	$1.0 \cdot C_{mp}$
(5) Maintenance (C_m)	$0.04 \cdot IFC$
(6) Supervision and support labor (C_s)	$0.3 \cdot (C_m + C_{mp})$
(7) Operative supplies	$0.15 \cdot C_m$
(8) Laboratory charges	$0.1 \cdot C_{mp}$
− Plant overhead, POC	$0.6 \cdot (C_m + C_{mp} + C_s)$
Additional costs, AC=ADM+R&D	
− Administrative, ADM	$0.15 \cdot C_{mp}$
− Research and development, R&D	$0.055 \cdot PC$

Table 5. Specific costs of reposition materials and utilities (C_{rm}^u)

Reposition materials and utilities	**Cost**	**Unit**	**Reference**
Electricity	0.072	\$/kWh	[29]
Low-pressure steam	0.01251	\$/kg	[50]
Cooling wáter	0.05093	\$/t	[50]
MEA make-up	1858.35	\$/t	[45]
Membrane reposition	10.0	\$/m^2	[29]

The manpower cost (C_{mp}) is estimated based on the guidelines given in Henao [51]. The estimated annual manpower costs to operate the membrane system, the chemical absorption process, and the final compression stage are 0.1089, 0.1927, and 0.2095 M$/yr., respectively.

The General Algebraic Modeling System (GAMS v. 23.6.5) [52] and the code CONOPT 3 (v. 3.14W) [53] were used to implement and solve the resulting NLP models, respectively. Since they are nonlinear and non-convex problems, the initialization strategy recently proposed by Mores at al. [31] for chemical absorption processes and that proposed by Arias et al. [22] for membrane systems were applied to overcome numerical convergence problems.

5. Results and discussion

Figure 3 shows the optimal TAC values obtained for both capture processes for feed CO_2 molar fraction values $x_{F,CO2}$ included in the range 0.04-0.44, with an interval of 0.01. As illustrated, this composition range comprises typical CO_2 concentrations of flue gases emitted from different plants such as natural gas and coal-fired power plants, refinery processes, cement and steel production plants, among other industries [54]. In addition, Table 6 presents the TAC and OPEX values computed for $x_{F,CO2}$ values which correspond to the limits of each sub-range.

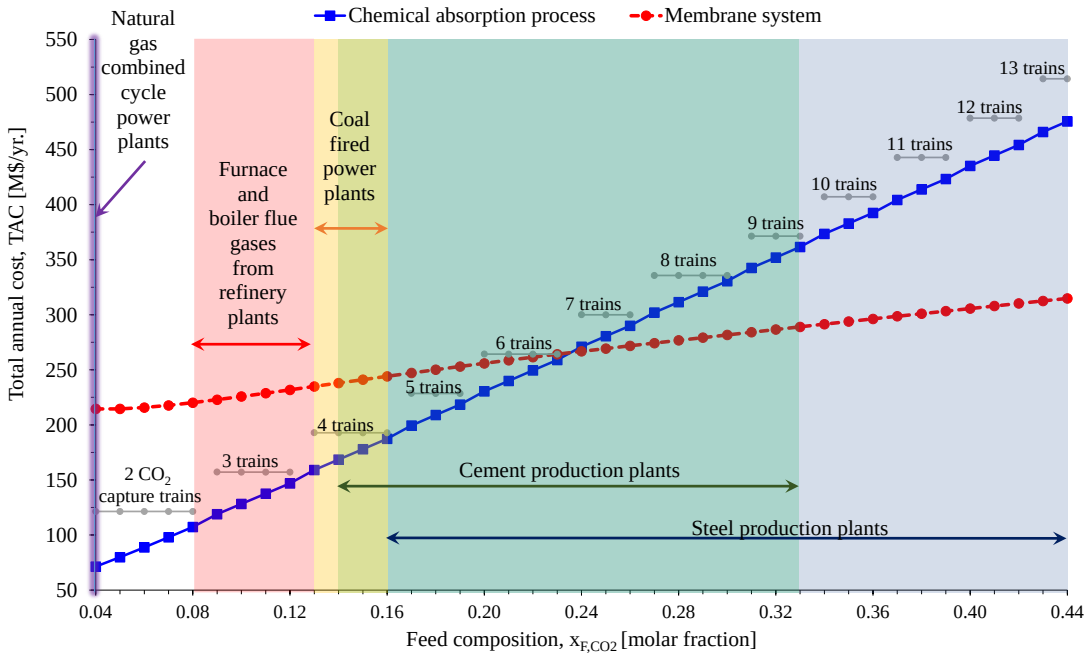

Figure 3. Optimal total annual cost (TAC) versus feed CO_2 composition ($x_{F,CO2}$) obtained for the membrane system and chemical absorption process (feed flow rate: 22.32 kmol/s; CO_2 recovery level: 90%; CO_2 purity level: ≥0.95).

As a first conclusion, it can be said that the best process –in terms of the TAC values– depends on the considered $x_{F,CO2}$ values, and that, for increasing $x_{F,CO2}$ values, the TAC value of the chemical absorption process increases more rapidly than that of the membrane-based systems; for example, for the typical CO_2 concentration values of natural gas combined cycle power plants (0.04-0.08), refinery processes (0.08-0.13), and coal-fired power plants (0.13-0.16), the chemical absorption process is always preferred in terms of TAC over the membrane system, and such preference becomes more evident with decreasing $x_{F,CO2}$ values. For the typical $x_{F,CO2}$ values of the cement production plants (0.14-0.33) and steel production plants (0.16-0.33), the chemical absorption process remains the cheapest technology up to around $x_{F,CO2}$=0.23, but the difference in TAC values between both processes decreases monotonically. At $x_{F,CO2}$=0.235, the TAC value obtained for both processes is practically the same. For $x_{F,CO2}$ values higher than 0.24, the membrane-based system shows TAC values lower than the chemical absorption process, and it becomes the preferred technology in terms of costs.

Also, it should be noted in Fig. 3 that the optimal number of CO_2 capture trains required by the chemical absorption process varies with the feed composition $x_{F,CO2}$. Indeed, for a specified 90% CO_2 recovery level, chemical absorption plants consisting of 2 to 13 absorption trains operating in parallel are required, depending on the $x_{F,CO2}$ value for a particular case.

Table 6 shows that the OPEX is the largest contributor to the TAC of both capture processes; it approximately represents between 64.9 and 74.1% of the TAC of the membrane system and between 78.2 and 86.9% of the TAC of the chemical absorption process. It can also be observed that the increase of the OPEX with increasing $x_{F,CO2}$ values (from 0.04 to 0.44) is more significant for the chemical absorption process (326.10 M$/yr., from 88.51 to 413.11 M$/yr.) than for the membrane system (88.68 M$/yr., from 144.58 to 233.26 M$/yr.). A similar qualitative behavior but of less quantitative importance was observed for the CAPEX and its contribution to the TAC of both processes.

The complete optimal solutions obtained for $x_{F,CO2}$=0.16 −where the chemical absorption process is preferred over the membrane system in terms of TAC−, for $x_{F,CO2}$=0.235 −where the TAC value of both processes is practically the same−, and for $x_{F,CO2}$=0.41 −where the membrane system is the preferred technology− are next presented. Tables 7 to 13 compare the optimal values of TAC, CAPEX, annualized CAPEX, OPEX, as well as the contribution of each cost item, between both processes. Figures 4 to 9 show the corresponding optimal operating conditions and sizes of all process units for the above-mentioned $x_{F,CO2}$ values.

Table 6. Cost distribution resulting for both capture processes for typical CO_2 compositions of industrial flue gases.

$X_{F,CO2}$	Membrane-based process		Amine-based absorption process	
	TAC (M$/yr.)	OPEX (% of TAC)	TAC (M$/yr.)	OPEX (% of TAC)
0.04[a]	214.55	64.87	71.24	78.22
0.08 - 0.13[b]	220.16 - 234.94	65.67 - 67.27	107.25 - 158.99	82.53 - 83.82
0.13 - 0.16[c]	234.94 - 244.14	67.27 - 68.28	158.99 - 187.38	83.82 - 84.79
0.14 - 0.33[d]	238.03 - 289.05	67.61 - 72.74	168.46 - 361.57	84.18 - 86.40
0.16 - 0.44[e]	244.14 - 314.84	68.28 - 74.09	187.38 - 475.61	84.79 - 86.86

[a] natural gas combined cycle power plants, [b] refinery plants, [c] coal-fired power plants, [d] cement plants, [e] steel plants.

The optimization results for $x_{F,CO2}$=0.16 presented in Table 7 indicate that the optimal TAC for the chemical absorption process with 4 absorption trains is 23.24% lower than that for the membrane-based system (187.38 vs. 244.14 M$/yr.). In both capture processes, the contribution of the OPEX to the TAC is more significant than the contribution of the annualized CAPEX: 84.79% vs. 15.21% in the amine-based absorption process, and 68.28% vs. 31.72% in the membrane-based process.

Table 7. TAC, OPEX, and annualized CAPEX

	$x_{F,CO2}$ = 0.16		$x_{F,CO2}$ = 0.235		$x_{F,CO2}$ = 0.41	
	Amine	**Memb.**	**Amine**	**Memb.**	**Amine**	**Memb.**
Total annual cost, TAC (M$/yr.)	187.38	244.14	266.36	265.56	444.76	308.00
Annualized capital expenditures, annualized CAPEX (M$/yr.)	28.50	77.43	38.63	77.34	59.01	80.86
Operating expenditures, OPEX (M$/yr.)	158.88	166.71	227.73	188.21	385.74	227.14

Table 8. Capital expenditures (CAPEX)

	$x_{F,CO2}$ = 0.16		$x_{F,CO2}$ = 0.235		$x_{F,CO2}$ = 0.41	
	Amine	**Memb.**	**Amine**	**Memb.**	**Amine**	**Memb.**
Capital expenditures, CAPEX (M$)	304.21	826.56	412.37	825.65	629.96	863.13
Investment in fixed capital, IFC	225.34	612.27	305.46	611.60	466.64	639.36
Working investment	56.34	153.07	76.36	152.90	116.66	159.84
Start-up cost	22.53	61.23	30.55	61.16	46.66	63.94

353

354 **Table 9**. Investment in fixed capital (direct and indirect manufacturing costs)

	$x_{F,CO2}$ = 0.16		$x_{F,CO2}$ = 0.235		$x_{F,CO2}$ = 0.41	
	Amine	**Memb.**	**Amine**	**Memb.**	**Amine**	**Memb.**
Invest. in fixed capital, IFC=DMC+IMC (M$)	225.34	612.27	305.46	611.60	466.64	639.36
Direct manufacturing costs, DMC	163.88	445.28	222.15	444.80	339.37	464.99
Equipment acquisition cost, C_{inv}	60.97	165.66	82.65	165.47	126.26	172.99
Equipment installation	32.19	87.47	43.64	87.37	66.66	91.34
Piping	24.39	66.26	33.06	66.19	50.50	69.19
Instrumentation and control	12.19	33.13	16.53	33.09	25.25	34.60
Service facilities	12.19	33.13	16.53	33.09	25.25	34.60
Electrical	6.71	18.22	9.09	18.20	13.89	19.03
Building and services	6.10	16.57	8.26	16.55	12.63	17.30
Yard improvements	6.10	16.57	8.26	16.55	12.63	17.30
Land	3.05	8.28	4.13	8.27	6.31	8.65
Indirect manufacturing costs, IMC	61.46	166.98	83.31	166.80	127.27	174.37
Engineering	16.39	44.53	22.22	44.48	33.94	46.50
Construction expenses	16.39	44.53	22.22	44.48	33.94	46.50
Contractor's fee	0.82	2.23	1.11	2.22	1.70	2.32
Contingencies	27.86	75.70	37.77	75.62	57.69	79.05

355

356

357 **Table 10**. Operating expenditures (OPEX)

	$x_{F,CO2}$ = 0.16		$x_{F,CO2}$ = 0.235		$x_{F,CO2}$ = 0.41	
	Amine	**Memb.**	**Amine**	**Memb.**	**Amine**	**Memb.**
Operating expenditures, OPEX (M$/yr.)	158.88	166.71	227.73	188.21	385.74	227.14
Total production costs (M$/yr.)	150.54	157.97	215.80	178.36	365.58	215.25
− Direct production costs	136.43	120.26	196.79	140.68	336.70	175.88
Reposition material and utilities, C_{rm}	122.80	84.30	178.51	104.76	309.08	138.35
Operation manpower, C_{mp}	0.40	0.32	0.40	0.32	0.40	0.32
Maintenance, C_m	9.01	24.49	12.22	24.46	18.67	25.57
Supervision and support labor, C_s	2.82	7.44	3.79	7.43	5.72	7.77
Operation supplies	1.35	3.67	1.83	3.67	2.80	3.84
Laboratory charges	0.04	0.03	0.04	0.03	0.04	0.03
− Fixed charges	6.76	18.37	9.16	18.35	14.00	19.18
Local taxes	4.51	12.25	6.11	12.23	9.33	12.79
Insurance	2.25	6.12	3.05	6.12	4.67	6.39
− Plant overhead	7.34	19.35	9.84	19.33	14.87	20.20
Additional costs (M$/yr.)	8.34	8.74	11.93	9.86	20.17	11.89
− Administrative	0.06	0.05	0.06	0.05	0.06	0.05
− Research and development	8.28	8.69	11.87	9.81	20.11	11.84

358

359

360

Table 11. Equipment acquisition cost (C_{inv}) for the amine-based process and CO_2 final compression

	$x_{F,CO2}$ = 0.16	$x_{F,CO2}$ = 0.235	$x_{F,CO2}$ = 0.41
Equipment acquisition cost, C_{inv} (M$)	**60.97**	**82.65**	**126.26**
Chemical absorption with amines	**38.98**	**54.88**	**87.46**
Absorber	12.93	15.63	22.29
(column/packing)	(3.95/8.98)	(5.48/10.15)	(8.51/13.78)
Heat exchanger (AAHE)	6.79	10.34	16.97
Reboiler (REB)	5.73	8.99	15.49
Heat exchangers (COND)	4.68	7.25	12.53
Regenerator	2.95	4.51	7.91
(column /packing)	(1.54/1.41)	(2.46/2.05)	(4.28/3.62)
Heat exchanger (AWHE)	2.15	2.82	3.86
Water tank (WTK)	1.75	2.76	4.78
Blower (BLOW)	1.59	1.95	2.54
MEA tank (ATK)	0.28	0.44	0.76
Rich amine pump (RAP)	0.12	0.19	0.33
CO_2 final compression	**21.99**	**27.77**	**38.79**
Compressors (COMP)	17.24	21.76	30.40
CO_2 pump (CO_2P)	3.67	4.62	6.46
Heat exchangers (IC)	1.08	1.38	1.94

Table 12. Equipment acquisition cost (C_{inv}) for the membrane-based process and CO_2 final compression

	$x_{F,CO2}$ = 0.16	$x_{F,CO2}$ = 0.235	$x_{F,CO2}$ = 0.41
Equipment acquisition cost, C_{inv} (M$)	**165.66**	**165.47**	**172.99**
Membrane system	**142.20**	**135.92**	**131.72**
Compressor (COM1)	40.53	41.27	37.74
Expander (EXP)	30.96	29.78	24.07
Membrane (MEM1)	27.85	31.49	34.19
Vacuum pump (PUMP1)	19.43	5.32	0.00
Compressor (COM2)	17.87	21.22	23.55
Membrane (MEM2)	3.18	4.43	9.95
Heat exchangers (HE1)	1.29	1.32	1.33
Heat exchangers (HE2)	0.63	0.75	0.90
Heat exchangers (HE3)	0.48	0.33	0.00
CO_2 final compression	**23.46**	**29.56**	**41.26**
Compressors (COMP)	18.75	23.63	32.98
CO_2 pump (CO_2P)	3.74	4.72	6.58
Heat exchangers (IC)	0.96	1.21	1.69

Table 13. Reposition material and utility cost (C_{rm})

	$x_{F,CO2}$ = 0.16		$x_{F,CO2}$ = 0.235		$x_{F,CO2}$ = 0.41	
	Amine	**Memb.**	**Amine**	**Memb.**	**Amine**	**Memb.**
Reposition mat. and utilities, C_{rm} (M$/yr.)	**122.80**	**84.30**	**178.51**	**104.76**	**309.08**	**138.35**
Electricity	23.44	79.86	33.16	99.54	56.16	132.07
Low pressure steam	77.46	–	113.23	–	196.68	–
Cooling water	6.21	3.27	9.04	3.86	15.95	4.61
MEA make-up	15.69	–	23.08	–	40.28	–
Membrane reposition	–	1.17	–	1.36	–	1.67

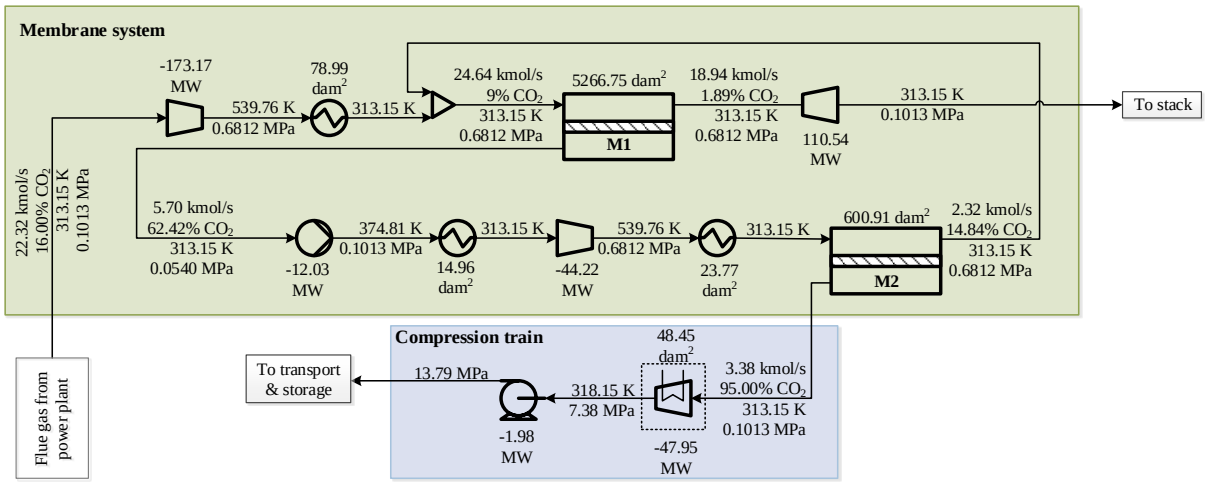

Figure 4. Optimal solution for the membrane-based process for treating a flue gas stream with a fresh feed CO_2 composition $x_{F,CO2}$ of 0.16 mole fraction.

According to Fig. 4, the membrane-based process requires a total membrane area of 5867.66 dam^2 (5266.75 dam^2 in the first stage and 600.91 dam^2 in the second one), which represents 18.73% of the total equipment acquisition cost C_{inv} (31.03 of 165.66 M$ including the CO_2 final compression cost) as shown in Table 12. The electric power capacity required in the first membrane stage for feed compression is 173.17 MW and for vacuum is 12.03 MW, the required in the second stage for permeate compression is 44.22 MW, and the required in the final compression stage is 49.93 MW (47.95 MW in the compressor and 1.98 MW in the CO_2 pump), resulting in a total capacity of 279.35 MW which represents 60.55% of the C_{inv} (100.32 of 165.66 M$). The power recovered from the retentate stream in the expander EXP is 110.54 MW, requiring an investment of 30.96 M$ which represents 18.69% of the C_{inv}.

The total heat transfer area required in the membrane stages is 117.72 dam^2 and in the compression stage is 48.45 dam^2, which represent only 2.03% of the C_{inv} (3.36 of 165.66 M$). In addition, the results presented in Table 12 allows seeing that the first membrane stage (formed by

MEM1, COMP1, PUMP1, HE1, and HE3) is the largest contributor to the C_{inv}, followed by the expander EXP and the second membrane stage (MEM2, COM2, HE2). The compressors of the first and second membrane stages are significantly more expensive than the membranes itself (40.53 vs. 27.85 M$ and 17.87 vs. 3.18 M$, respectively). Finally, the investment required by the second stage (21.67 M$) is similar to the investment required by the compression stage (23.46 M$). Also, similar investments are required by the vacuum pumps PUMP1 and compressors COM2 (19.43 and 17.87 M$).

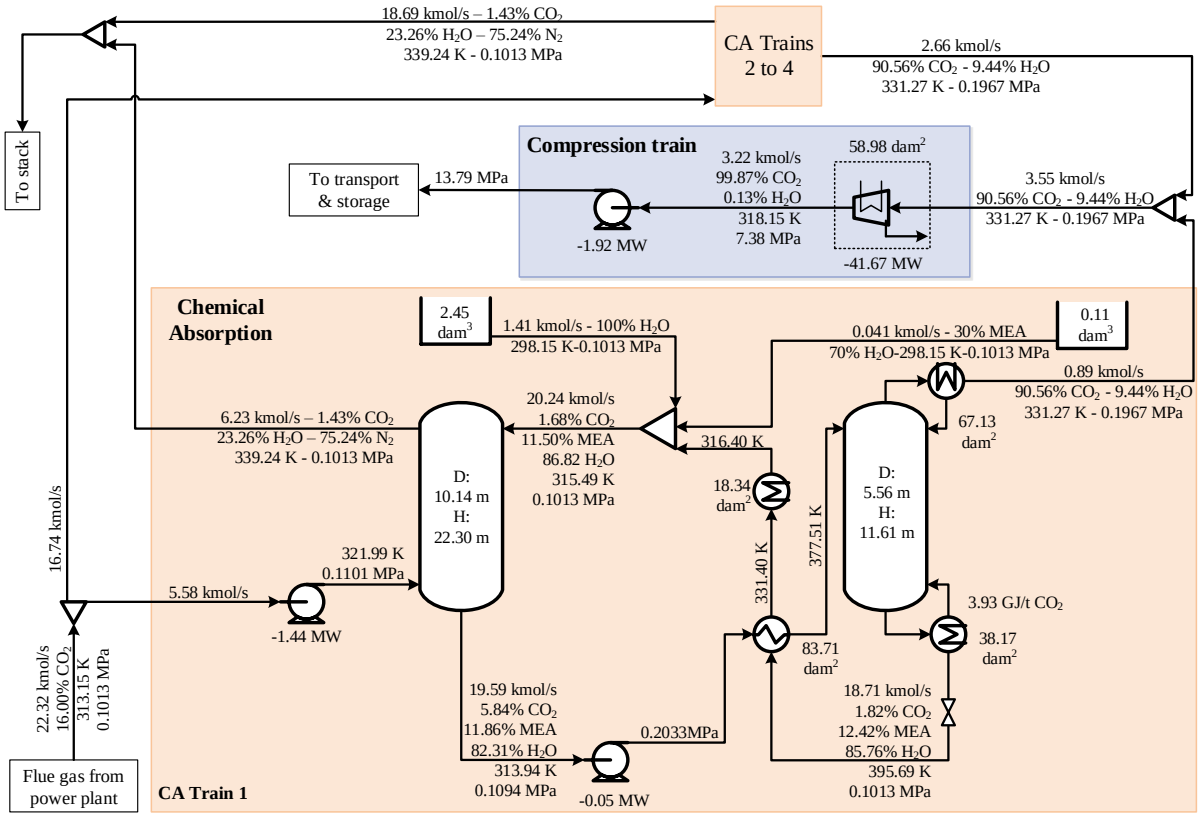

Figure 5. Optimal solution for the amine-based absorption process for treating a flue gas stream with a fresh feed CO_2 composition $x_{F,CO2}$ of 0.16 mole fraction.

Regarding the optimization results for the chemical absorption process, Figs. 3 and 5 show that the optimal process configuration consists of 4 capture trains. The optimal diameter and packing height of the absorption columns are 10.14 m and 22.30 m, respectively (Fig. 5), implying a total packing volume of 7197.92 m^3 (1799.48 m^3 each) which represents 14.73% of the equipment acquisition cost C_{inv} (8.98 of 60.97 M$), as shown in Table 11. Taking into account the packing material and the columns, the 4 absorbers are the process units that contribute most to the C_{inv}, with 21.21% (12.93 of 60.97 M$). They are followed by the amine heat exchangers AAHE and reboilers

REB, which contribute 11.14% and 9.39%, respectively. The amine-amine heat exchangers require a total area of 334.82 dam^2 (83.71 dam^2 each) to transfer a total heat load of 453.98 MW (113.50 MW each) with a driving force of 17.82 K. While the reboilers require a total heat transfer area of 152.68 dam^2 (38.17 dam^2 each) to transfer in total 15.70 GJ/t CO_2. This heat load is supplied with 261.84 kg/s of saturated steam at 4.44 atm and a driving force value of 26.73 K. The fourth largest contributors to the C_{inv} are the condensers COND with 4.68 M$, followed by the regenerators and amine-water heat exchangers AWHE with 2.95 M$ and 2.15 M$, respectively.

The total heat load in the condensers is 350.48 MW, which is rejected with 3351.3 kg/s of cooling water, a total heat transfer area of 268.53 dam^2 (67.13 dam^2 each), and a driving force value of 46.76 K. With respect to the amine regeneration section, the optimal diameter and packing height of the regeneration columns are 5.56 m and 11.61 m, respectively (Fig. 5), resulting in a total packing volume of 1126.87 m^3 (281.72 m^3 each). It represents only 2.31% of the C_{inv} (1.41 of 60.97 M$). Taking into account the packing material and the columns, the 4 regenerators contribute to the C_{inv} with 4.84% (2.95 of 60.97 M$). Finally, the investments required by the blowers BLOW and water tanks WTK are similar (1.59 and 1.75 M$, respectively), which represent together 5.48% of the C_{inv}. The investments associated with the MEA tanks ATK and amine pumps RPA are 0.28 and 0.12 M$, respectively, with insignificant contributions to the C_{inv}.

The total electric power capacity required by the compression stage is 43.59 MW (41.67 MW by the compressor and 1.92 MW by the pump) which determines an investment of 20.91 M$, representing 34.30% of the C_{inv}.

When comparing the optimal TAC values between both processes for $x_{F,CO2}$=0.16 (Table 7), it can be observed that the difference in these values is mainly due to the annualized CAPEX rather than the OPEX values, which are both greater in the membrane process. Precisely, the annualized CAPEX obtained for the membrane process is more than twice the obtained for the chemical absorption process (77.43 vs. 28.50 M$/yr.). The difference in the OPEX values is less significant (166.71 vs. 155.88 M$/yr.).

The cost for electric power demanded by the membrane-based process represents 94.73% of the C_{rm}. It is much higher than that demanded by the amine-based process (79.86 vs. 23.44 M$/yr.) (Table 13), and it is close to the cost related to steam consumption for amine regeneration (79.86 vs. 77.46 M$/yr.). In the amine-based process, electricity and MEA make-up are the second and third contributors to the C_{rm} with 23.44 and 15.69 M$/yr., respectively. The cost required by the cooling water is twice compared to that required by the membrane-based process.

Regarding the optimization results obtained for $x_{F,CO2}$=0.41, it can be seen in Table 7 that the optimal TAC value for the membrane-based system is 30.75 % lower than the obtained for the chemical absorption system (308.00 vs. 444.76 M$), which is contrary to the behavior found for $x_{F,CO2}$=0.16. The optimal annualized CAPEX obtained for the membrane-based process is 37.03% greater than the obtained for the amine-based process (80.86 vs. 59.01 M$/yr.). But, unlike for $x_{F,CO2}$=0.16, the optimal OPEX value is 41.12% lower than the amine-based process, resulting in a decreasing value of TAC.

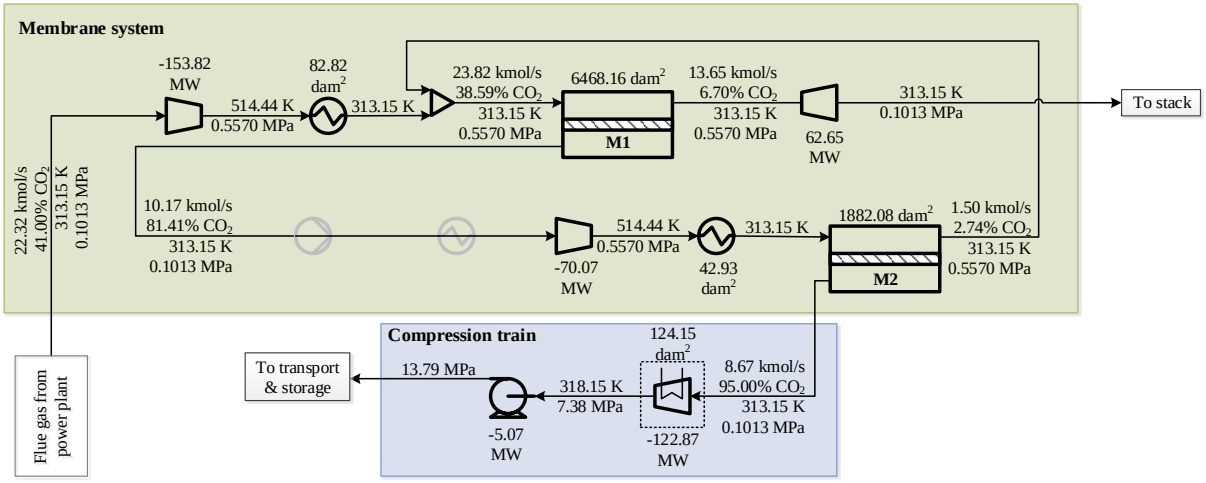

Figure 6. Optimal solution for the membrane-based process for treating a flue gas stream with a fresh feed CO_2 composition $x_{F,CO2}$ of 0.41 mole fraction.

The comparison of results in Table 7 indicates that the costs obtained for $x_{F,CO2}$=0.41 increase with respect to $x_{F,CO2}$=0.16 in both processes, but the increases in the chemical absorption process are more significant than the increases in the membrane-based process. Indeed, the OPEX increases by 219.03 M$/yr. and 60.43 M$/yr. for the amine- and membrane-based processes, respectively; and the annualized CAPEX increases by 30.52 M$/yr. and only 3.43 M$/yr. for the amine- and membrane-based processes, respectively.

Similar to $x_{F,CO2}$=0.16, Table 12 indicates that for $x_{F,CO2}$=0.41 the compressors COM1 and COM2 involved in the membrane stages contribute to the C_{inv} more than the area of membranes MEM1 and MEM2 (61.29 vs. 44.14 M$), with the particularity that the contribution of the membrane area in the first stage MEM1 is similar to the contribution of the compressor COM1 (37.74 vs. 34.19 M$), contrary to what happens with MEM2 and COM2 in the second stage (23.55 vs. 9.95 M$).

It is important to mention the trade-offs that exist between the operating pressure, the total power required for the separation, the power recovered in the expander, and the total membrane area

for $x_{F,CO2}$=0.16 and 0.41. Figure 4 shows that for $x_{F,CO2}$=0.16 the total power required by the membrane stages is 229.42 MW (12.03 MW required by the vacuum pumps) and the power recovered in the expander is 110.54 MW, resulting in a required net power of 118.88 MW (excluding the power required in compression stage). While for $x_{F,CO2}$=0.41 (Fig. 6) these values are 223.89 MW, 62.65 MW, and 161.39 MW, respectively. Thus, the net electric power required by the membrane process for $x_{F,CO2}$=0.41 is 42.51 MW higher than for $x_{F,CO2}$=0.16. This is because of the operating pressure for $x_{F,CO2}$=0.41 is lower than for $x_{F,CO2}$=0.16 (0.5570 vs. 0.6812 MPa) but implying a larger membrane area (8350.24 vs. 5867.66 dam^2). Also, it is worth to mention that no vacuum pump is required in the first stage, contrary to what was obtained for $x_{F,CO2}$=0.16. In this sense, the benefit of including a vacuum pump in the first membrane stage was investigated for the whole range of $x_{F,CO2}$ values examined. The optimization results (not shown) indicated that a vacuum pump is included in the optimal solutions corresponding to $x_{F,CO2}$ values lower than 0.24 and that the optimal ratio between the atmospheric and vacuum pressure values decrease from 5.02 for $x_{F,CO2}$=0.04 to 1.11 for $x_{F,CO2}$=0.24; for mole fractions higher than 0.24 this ratio is equal to 1.0 and, consequently, no vacuum is required.

Regarding the CO_2 final compression stage, the power required for $x_{F,CO2}$=0.41 is greater than for $x_{F,CO2}$=0.16 since it is necessary to compress a greater amount of CO_2 to the same pressure level (13.79 MPa). Then, it can be concluded that the higher is the flue gas CO_2 composition, the higher is the total membrane area, the higher is the power required to compress the CO_2 enriched stream, the lower is the operating pressure in the membrane stages, and the higher is the total net power required for separation only i.e. without considering the power required for the final CO_2 compression.

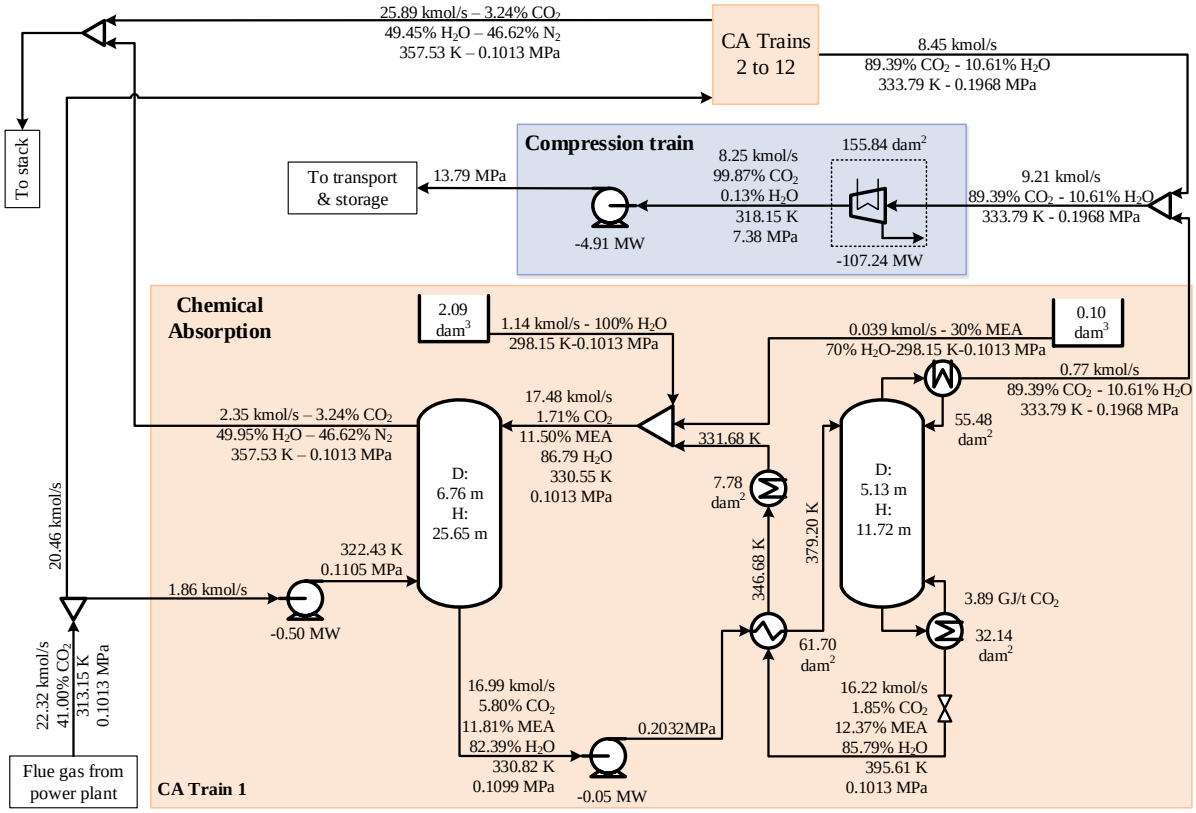

Figure 7. Optimal solution for the amine-based absorption process for treating a flue gas stream with a fresh feed CO_2 composition $x_{F,CO2}$ of 0.41 mole fraction.

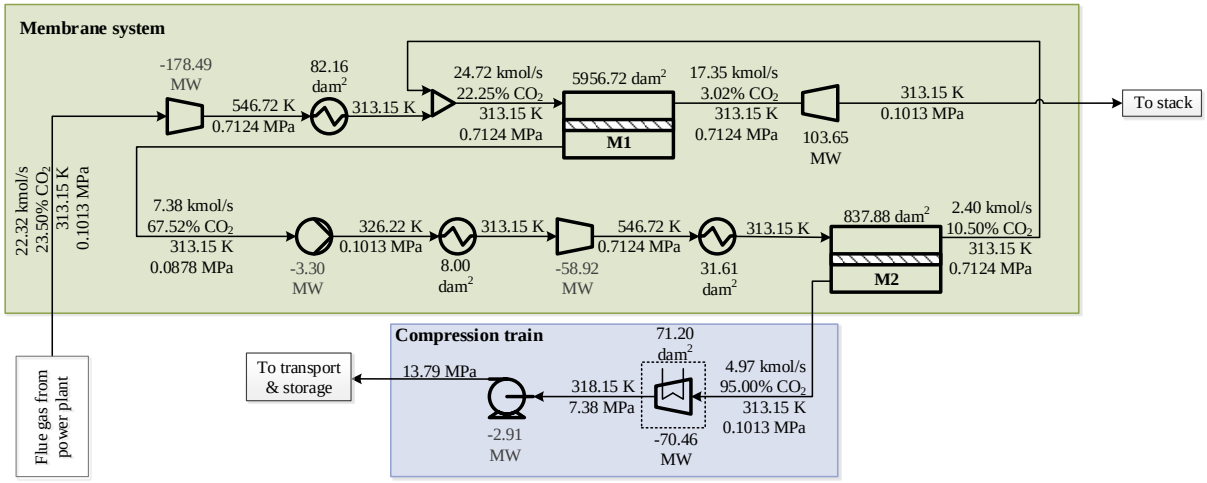

Figure 8. Optimal solution for the membrane-based process for treating a flue gas stream with a fresh feed CO_2 composition $x_{F,CO2}$ of 0.235 mole fraction.

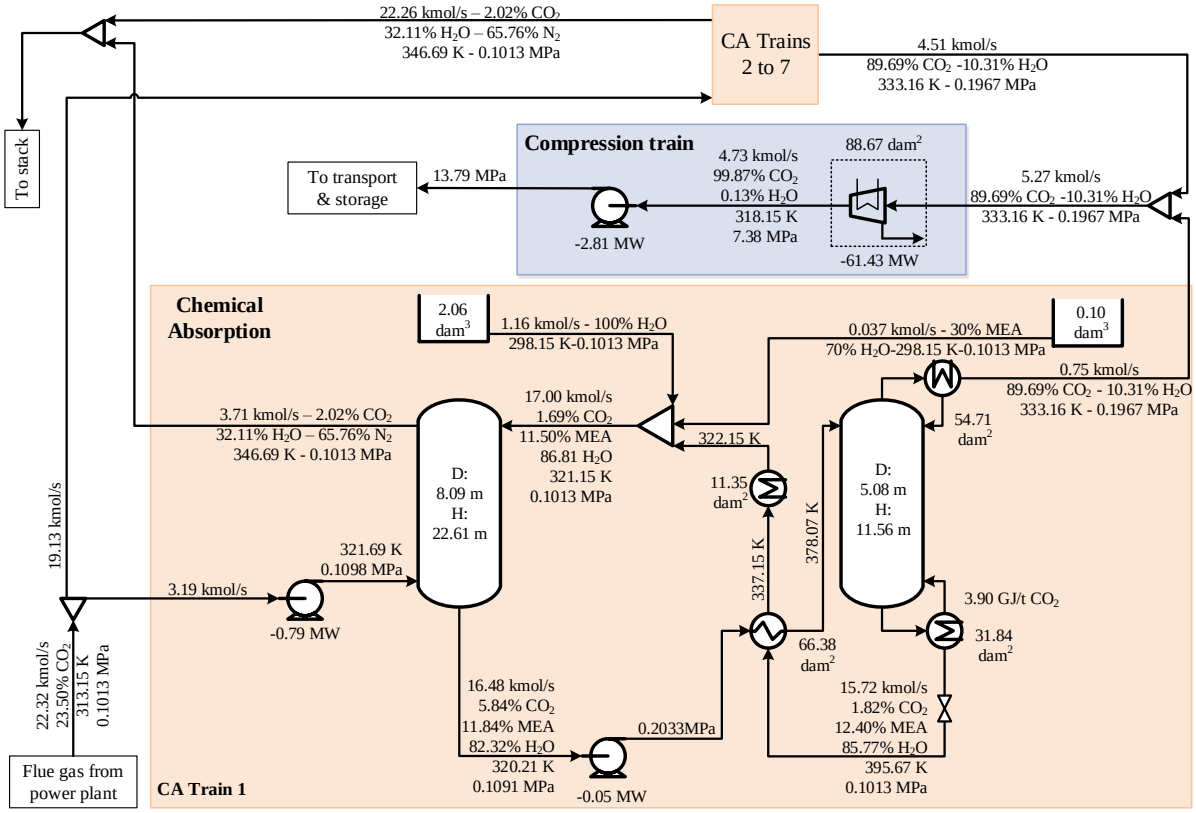

Figure 9. Optimal solution for the amine-based absorption process for treating a flue gas stream with a fresh feed CO_2 composition $x_{F,CO2}$ of 0.235 mole fraction.

Finally, it is interesting to mention some features of the optimal solutions obtained for both processes at $x_{F,CO2}$=0.235. As previously mentioned, the TAC obtained for both processes is almost the same (266.36 and 265.56 M$/yr. for the amine-based process and the membrane system, respectively –Table 7–). It should be noted that it is not exactly the same because the points plotted in Fig. 3 were systematically obtained by varying parametrically the $x_{F,CO2}$ value in 0.01; therefore, the coordinate corresponding to the crossing point, i.e. where both TAC values are identical, does not coincide exactly with a $x_{F,CO2}$ value used in an optimization run.

Figures 8 and 9 illustrate the optimal solutions obtained for both processes, which include the optimal values of flow rates, compositions, pressures, and temperatures of the process streams, and sizes of the process units. According to the values listed in Table 7, the optimal annualized CAPEX value for the amine-based process is twice that required by the membrane-based system, thus implying a lower OPEX value since both processes have practically the same TAC values. According to Table 9, the equipment acquisition cost C_{inv} represents 27.05% of the fixed capital investment IFC in both processes (82.65 of 305.46 M$ in the amine-based process, and 165.47 of

611.60 M$ in the membrane system), followed by the equipment installation and piping costs, which represent 14.28 and 10.82%, respectively, in both processes. Table 11 indicates that the chemical absorption process −excluding the compression stage− represents 66.40% of the C_{inv}, with the absorption columns (7 columns in total) being the largest contributor (15.63 of 54.88 M$). The final compression stage represents 33.60% of the C_{inv}, which is strongly influenced by the compressors which contribute with 78.35% (21.76 of 27.77 M$). On the other side, Table 12 indicates that the membrane system −excluding the compression stage− represents 82.14% of the C_{inv}, out of which 79.35% corresponds to process units involved in the first stage: COM1 (30.36%), MEM1 (23.16%), EXP (21.90%), and PUMP1 (3.91%).

Regarding the optimal OPEX values, Table 13 shows that, although the cost of electricity for the amine-based process is 3 times lower than that for the membrane system (33.16 vs. 99.54 M$/yr.), the OPEX value for the former is 70.0% higher than the latter (178.1 vs. 104.76 M$/yr.) due to the steam demand by amine regeneration (113.23 M$/yr.) and amine make-up (23.08 M$/yr.).

CONCLUSIONS

This paper compared the cost performance −in terms of the total annual cost, annual operation cost, and annualized investment cost− between two-stage membrane-based systems and amine-based chemical absorption processes for CO_2 capture from flue gas for the same design specifications. A wide range of CO_2 concentration values in the feed stream was considered, from 0.04 to 0.44 CO_2 mole fractions, which is representative of several CO_2-generating processes (natural gas and coal-fired power plants, refinery processes, and cement and steel production plants). As a result, the optimal process configuration, sizes of the process units, and operation conditions that minimize the total annual cost while satisfying a specified CO_2 recovery of 90% and a CO_2 purity of at least 0.95 were obtained for both processes. To this end, the nonlinear mathematical programming approach was applied, using gradient-based optimization algorithms.

Based on the considered cost model, the optimization results show that the chemical absorption process is always preferred in terms of TAC over the membrane system for the typical CO_2 concentration values of natural gas combined cycle power plants (0.04-0.08), refinery processes (0.08-0.13), and coal-fired power plants (0.13-0.16), and that such preference becomes more noticeable with decreasing $x_{F,CO2}$ values. For the typical $x_{F,CO2}$ values of the cement production plants (0.14-0.33) and steel production plants (0.16-0.33), the chemical absorption process remains the cheapest technology only up to about $x_{F,CO2}$=0.23 since at $x_{F,CO2}$=0.235 the TAC value obtained for both processes is practically the same. For $x_{F,CO2}$ values higher than 0.24, the membrane-based

system shows TAC values lower than the chemical absorption process, and it becomes the preferred technology in terms of costs. For instance, for $x_{F,CO2}$=0.16, the optimal TAC obtained for the amine-based process is 23.24% lower than that for the membrane-based system; conversely, for $x_{F,CO2}$=0.41, the optimal TAC obtained for the membrane-based system is 30.75% lower than that for the chemical absorption process.

The proposed optimization models constitute a valuable decision-support tool for designing, simulating and optimizing amine-based chemical absorption processes and membrane-based systems for post-combustion CO_2 capture, and the obtained results can serve as a guide to assist in selecting the best between both technologies, in terms of cost, for a particular industrial case.

In addition, the obtained results motivate to continue the study of alternative process configurations for CO_2 capture in order to reduce costs. In this sense, hybrid processes combining membranes with chemical absorption processes may offer cost-effective alternatives to the standalone processes. Several hybrid systems will be investigated in terms of efficiency and cost. To this end, a superstructure-based optimization approach using the mathematical models presented in this paper will be proposed.

Acknowledgements

The financial support from the Consejo Nacional de Investigaciones Científicas y Técnicas (CONICET) and the Facultad Regional Rosario of the Universidad Tecnológica Nacional from Argentina are gratefully acknowledged.

Nomenclature

Symbols

AC: total additional cost (M$/yr.).
CAPEX: capital expenditures (M$).
CRF: capital recovery factor (dimensionless).
C_{inv}: total equipment acquisition cost (M$).
C_{inv}^{k}: individual acquisition cost of the pieces of equipment (k) (M$).
C_m: cost of maintenance (M$/yr.).
C_{mp}: cost of manpower (M$/yr.).
C_{rm}: cost of raw materials and utilities (M$/yr.).
C_{rm}^{u}: specific cost of raw materials and utilities ($/t, $/GW).
C_S: supervision and support labor (M$/yr.).
DMC: total direct manufacturing cost (M$).
DPC: direct production costs (M$/yr.).
f_1, f_2, f_3: economic indexes (dimensionless).
FC: fixed charge (M$/yr.).
g_t: set of inequality constraints t.
HTU: height of a transfer unit (dimensionless).

h_s: set of equality constraints s.
i: interest rate (%).
IFC: investment in fixed capital (M$).
IMC: total indirect manufacturing cost (M$).
m^u: annual consumption of raw materials and utilities (kg/yr.).
NTU: number of transfer units (dimensionless).
n: project lifespan (yr.).
OPEX: operating expenditures (M$/yr.).
PC: production cost (M$/yr.).
POC: plant overhead (M$/yr.).
R_{CO2}: CO_2 recovery (%).
TAC: total annual cost (M$/yr.).
WI: working investment (M$).
X^k: size of the process unit k (dam^2, MW, m^3).
$x_{CO2,F}$: CO_2 concentration in the feed stream (mole fraction).

Acronyms
CCS: CO_2 capture and storage.
CCU: CO_2 capture and utilization.
GAMS: General Algebraic Modeling System.
HTU: height of a transfer unit.
NLP: nonlinear programming.
NTU: number of transfer units.

Abbreviations
AAHE: amine-amine heat exchanger.
AWHE: amine-water cooler.
ABS: absorption column.
IC: heat exchangers (intercooling in the compression stage).
ATK: amine tank.
BLOW: blower.
COM1, *COM2*: compressor in the first and second membrane stage.
COMP: compressor in the compression stage.
COND: condenser.
EXP: expander.
MEA: monoethanolamine.
MEM1, *MEM2*: first and second membrane stages.
P1: CO_2-enriched permeate stream.
PUMP1, *CO_2P*: pump.
R1: CO_2-lean retentate stream.
RAP: rich amine solution pump.
REB: reboiler.
REG: regeneration column.
WTK: water tank.

Appendix A. Membrane-based system

Figures A1 and A2 illustrate, respectively, the entire membrane-based process and the nomenclature used to derive the mathematical model of each membrane stage (MEM1 and MEM2).

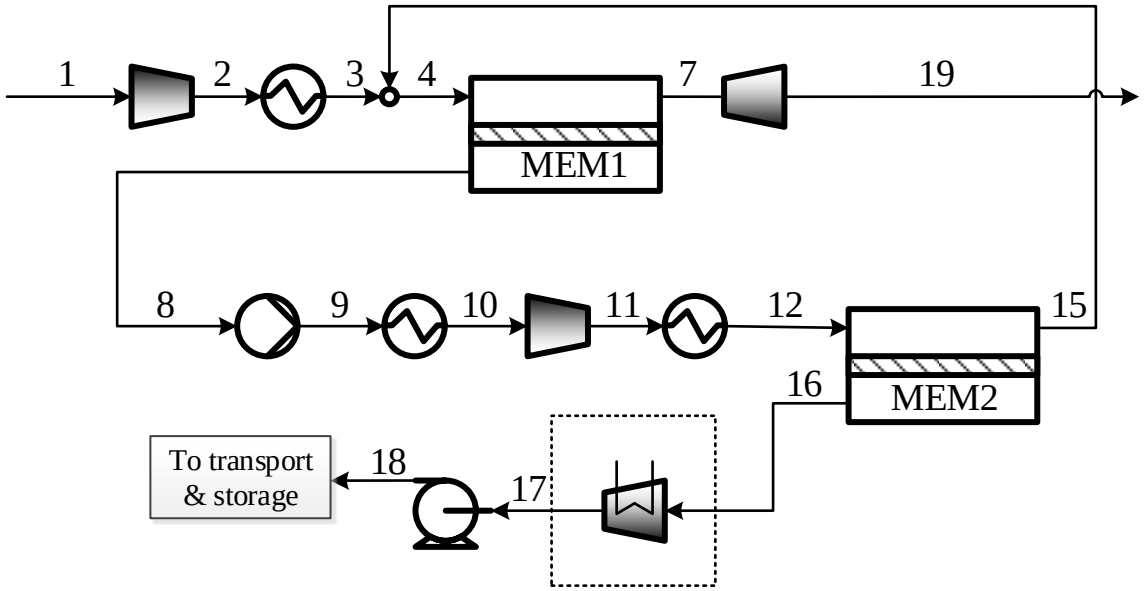

Figure A1. Schematic of the membrane-based process.

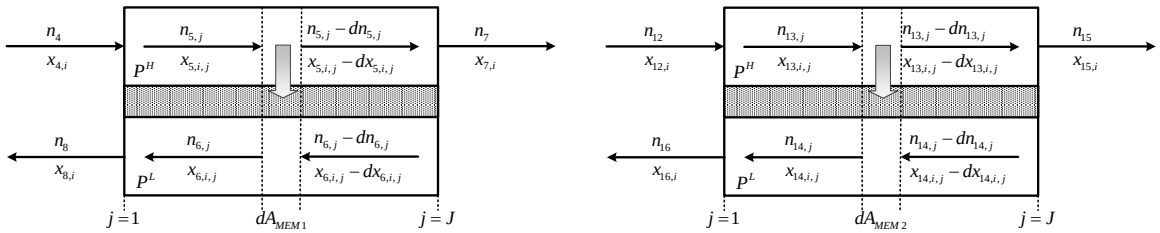

Figure A2. Schematic representation and nomenclature associated with the stages MEM1 and MEM2 (counter-current flow configuration).

A.1 Mass balances

The differential ordinary equation that describes the mass balance for the component *i* around a differential volume element of area ΔA in steady state is expressed in Eq. (A1):

$$-d\frac{n_7 \cdot x_{7,i}}{dA_{MEM\,1}} = \xi_i \cdot \left(P^H \cdot x_{7,i} - P^L \cdot x_{8,i}\right) \quad \text{(A1)}$$

where ξ_i is the permeance of component *i*, A is the membrane surface area, and P^H and P^L are the retentate and permeate side pressures, respectively.

The set of algebraic equations obtained for the discretization of the ODE (A1) by applying the backward finite difference method (BFDM) is expressed in Eq. (A2) to (A4):

$$-d\frac{n_7 \cdot x_{7,i}}{dA_{MEM1}} = \xi_i \cdot \left(P^H \cdot x_{7,i} - P^L \cdot x_{8,i}\right), \quad i = CO_2, N_2 \tag{A2}$$

$$\frac{1}{2}\frac{(J-1)}{A_{MEM1}}\left(-n_{5,j} \cdot x_{5,i,j} + n_{5,j+2} \cdot x_{5,i,j+2}\right) + \xi_i \left(P^H \cdot x_{5,i,j+1} - P^L \cdot x_{6,i,j+1}\right) = 0, \;\; j = 1; i = CO_2, N_2 \tag{A3}$$

$$\begin{aligned} &\frac{1}{2}\frac{(J-1)}{A_{MEM1}} \cdot \left(n_{5,j} \cdot x_{5,i,j} - 4 \cdot n_{5,j+1} \cdot x_{5,i,j+1} + 3 \cdot n_{5,j+2} \cdot x_{5,i,j+2}\right) + && j = 1, \ldots, J-2 \\ &\xi_i \cdot \left(P^H \cdot x_{5,i,j+2} - P^L \cdot x_{8,i,j+2}\right) = 0 && i = CO_2, N_2 \end{aligned} \tag{A4}$$

where the subscript *j* represents the discretization points of the spatial domain.

The relationships between the flow rate and composition in the permeate stream in each discretization point are given by the following constraints:

$$n_{5,j} - n_{5,j=J} - n_{6,j} = 0, \quad \forall j \tag{A5}$$

$$n_{5,j} \cdot x_{5,i,j} - n_{5,j=J} \cdot x_{5,i,j=J} - n_{6,j} \cdot x_{6,i,j} = 0, \quad \forall i, \forall j \tag{A6}$$

$$\sum_{i=1}^{2} x_{5,i,j} = 1, \quad \forall j \tag{A7}$$

$$\sum_{i=1}^{2} x_{6,i,j} = 1, \quad \forall j \tag{A8}$$

The stage cut φ_j, which represents the fraction of the feed flow rate that permeates at the discretization point j of the membrane, is expressed as:

$$\varphi_{j,MEM1} \cdot n_{5,j=1} - n_{5,j=1} + n_{5,j} = 0, \quad \forall j \tag{A9}$$

Also, the following total and component mass balances in both membrane stages are considered:

$$n_4 = n_7 + n_8 \tag{A10}$$

$$n_4 \cdot x_{4,i} = n_7 \cdot x_{7,i} + n_8 \cdot x_{8,i}, \quad i = CO_2, N_2 \tag{A11}$$

667

$$n_{12} = n_{15} + n_{16} \quad \text{(A12)}$$

$$n_{12} \cdot x_{12,i} = n_{15} \cdot x_{15,i} + n_{16} \cdot x_{16,i}, \quad i = CO_2, N_2 \quad \text{(A13)}$$

668 For an easier model implementation, the model variables that do not involve the index "j"
669 used for discretization are defined to refer the inlet and outlet flow rate and composition in each stage
670 (left-hand side), which are related to the discretized variables (right-hand side) as follows:

$$n_4 = n_{5,j}, \quad j = 1 \quad \text{(A14)}$$

$$n_8 = n_{6,j}, \quad j = 1 \quad \text{(A15)}$$

$$n_7 = n_{5,j}, \quad j = J \quad \text{(A16)}$$

$$x_{4,i} = x_{5,i,j}, \quad i = CO_2, N_2; j = 1 \quad \text{(A17)}$$

$$x_{8,i} = x_{6,i,j}, \quad i = CO_2, N_2; j = 1 \quad \text{(A18)}$$

$$x_{7,i} = x_{5,i,j}, \quad i = CO_2, N_2; j = J \quad \text{(A19)}$$

$$n_{12} = n_{13,j}, \quad j = 1 \quad \text{(A20)}$$

$$n_{16} = n_{14,j}, \quad j = 1 \quad \text{(A21)}$$

$$n_{15} = n_{13,j}, \quad j = J \quad \text{(A22)}$$

$$x_{12,i} = x_{13,i,j}, \quad i = CO_2, N_2; j = 1 \quad \text{(A23)}$$

$$x_{16,i} = x_{14,i,j}, \quad i = CO_2, N_2; j = 1 \quad \text{(A24)}$$

$$x_{15,i} = x_{13,i,j}, \quad i = CO_2, N_2; j = 1 \quad \text{(A25)}$$

671

672 Similar equations presented below are proposed for the membrane stage MEM2.

673

674 B.2 Power requirements

675 The power W_{MEM1} required for compressing the process feed is estimated by Eq. (A26):

$$W_{MEM1} = \frac{n_1}{\eta_C} \cdot \left(\frac{\gamma}{\gamma - 1} \right) \cdot R \cdot T_1 \cdot \left[\left(\frac{P^H}{P^L} \right)^{\frac{\gamma-1}{\gamma}} - 1 \right] \quad \text{(A26)}$$

where the relationship between P^H and T_2 is given by Eq. (A27):

$$\frac{T_2}{T_1} = \left(\frac{P^H}{P^L} \right)^{\frac{\gamma}{\gamma-1}} \quad \text{(A27)}$$

The power W_{MEM2} required for compressing the feed stream of the 2nd membrane stage is estimated by Eq. (A28):

$$W_{MEM2} = \frac{n_{10}}{\eta_C} \cdot \left(\frac{\gamma}{\gamma - 1} \right) \cdot R \cdot T_{10} \cdot \left[\left(\frac{P^H}{P^L} \right)^{\frac{\gamma-1}{\gamma}} - 1 \right] \quad \text{(A28)}$$

The power W_E recovered through an isothermal expansion of the retentate stream is calculated by Eq. (A29):

$$W_E = \frac{n_7}{\eta_E} \cdot R \cdot T_7 \cdot \ln \left(\frac{P^H}{P^L} \right) \quad \text{(A29)}$$

B.3 Energy balances

The required amount of cooling water in each heat exchanger can be obtained from Eqs. (A30) and (A31):

$$n_{cw,MEM1,1} \cdot c_P^{cw} \cdot \left(T_{cw,MEM1,2} - T_{cw,MEM1,2} \right) = n_2 \cdot c_P^g \cdot \left(T_2 - T_3 \right) \quad \text{(A30)}$$

$$n_{cw,MEM2} \cdot c_P^{cw} \cdot \left(T_{cw,MEM2,2} - T_{cw,MEM2,1} \right) = n_{11} \cdot c_P^g \cdot \left(T_{11} - T_{12} \right) \quad \text{(A31)}$$

B.4 Heat transfer areas

The heat transfer area for removing the heat generated to compress the process feed (HTA_{MEM1}) and the permeate stream in a stage *s* (HTA_{MEM2}) are estimated by Eqs. (A32) and (A33), respectively:

$$HTA_{MEM1} = \frac{n_{cw,MEM1} \cdot c_P^{cw} \cdot \left(T_{cw,2,MEM1} - T_{cw,1,MEM1} \right)}{U \cdot LMTD_{MEM1}} \quad \text{(A32)}$$

$$HTA_{MEM2} = \frac{n_{cw,MEM2} \cdot c_P^{cw} \cdot \left(T_{cw,1,MEM2} - T_{cw,2,MEM2} \right)}{U \cdot LMTD_{MEM2}} \quad \text{(A33)}$$

689 The logarithmic mean temperature difference *LMTD*, which is given by Eqs. (A34) and
690 (A35):

$$LMTD_{MEM\,1} = \frac{\left(T_2 - T_{cw,MEM\,1,2}\right) - \left(T_3 - T_{cw,MEM\,1,1}\right)}{\ln \dfrac{\left(T_2 - T_{cw,MEM\,1,2}\right)}{\left(T_3 - T_{cw,MEM\,1,1}\right)}} \tag{A34}$$

$$LMTD_{MEM\,2} = \frac{\left(T_{11} - T_{cw,MEM\,2,2}\right) - \left(T_{12} - T_{cw,MEM\,2,1}\right)}{\ln \dfrac{\left(T_{11} - T_{cw,MEM\,2,2}\right)}{\left(T_{12} - T_{cw,MEM\,2,1}\right)}} \tag{A35}$$

691 B.5 Performance variables

692 The total membrane stage area *TMA* is computed by Eq. (A36) and the total heat transfer area
693 *THTA* by Eq. (A37):

$$TMA = \sum_{s} MA_S, \quad s = MEM\,1, MEM\,2 \tag{A36}$$

$$THTA = \sum_{S} HTA_S, \quad s = MEM\,1, MEM\,2 \tag{A37}$$

694 The total power requirement TW is computed as follows:

$$TW = W_{MEM\,1} + W_{MEM\,2} + W_{Final\ Compression} \tag{A38}$$

695 where $W_{\text{Final Compression}}$ refers to the work required for the final compression.
696 Then, the total net power TNW is given by:

$$TNW = TW - W_E \tag{A39}$$

697
698
699 **Appendix B. Amine-based chemical absorption process**

700 Figures B1 and B2 illustrate, respectively, the entire amine-based chemical process and a
701 generic absorption column. Figure B3 includes the nomenclature used to derive the mathematical
702 model.

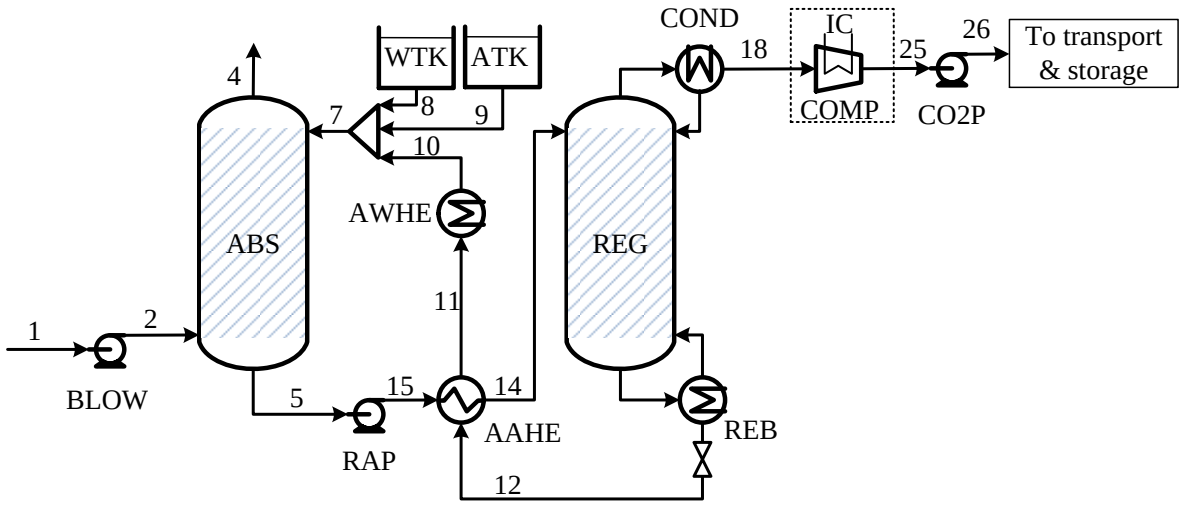

703

704 **Figure B1.** Schematic of the amine-based chemical absorption process.

705

706

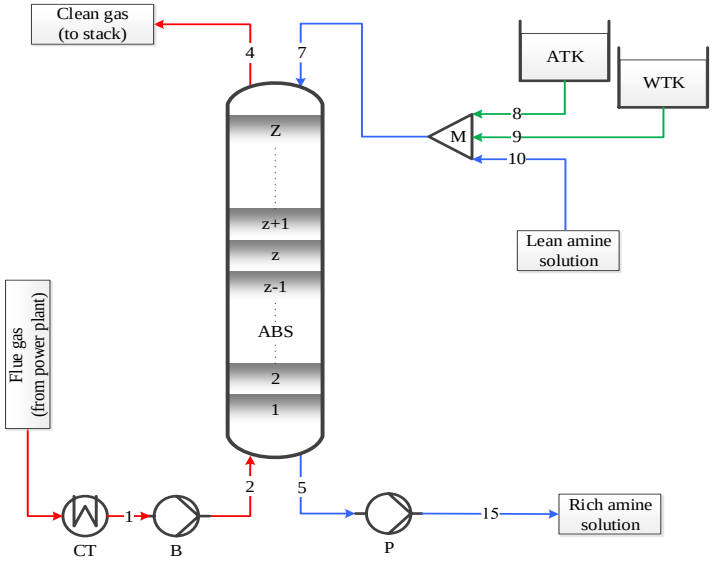

707

708 **Figure B2.** Schematic of the absorption process.

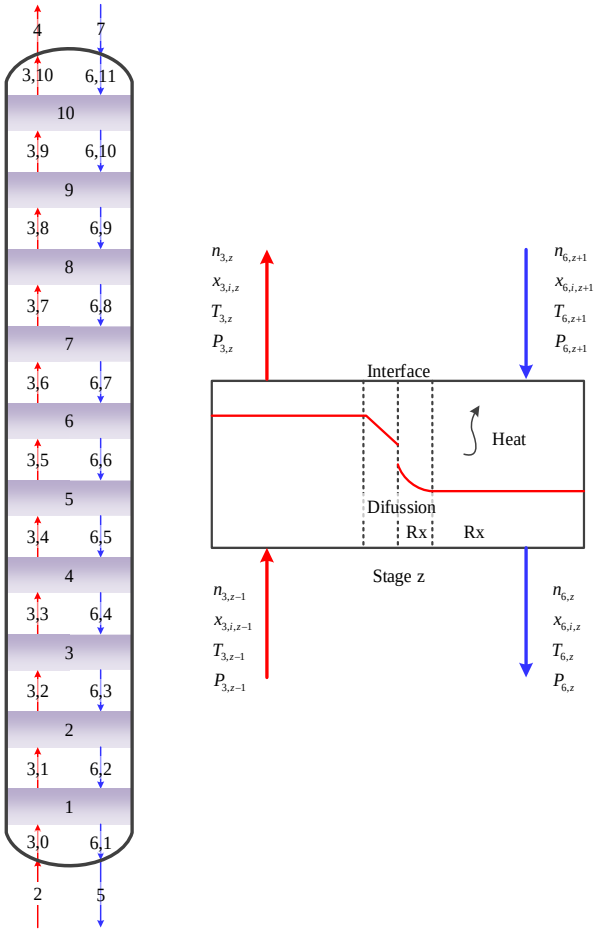

Figure B3. Schematic of a generic stage z of the absorption column.

As shown in Figs. B2 and B3, the gas stream #2 (and thereby #3) goes up from stage z−1 to stage z and the amine solution stream #7 (and thereby #6) flows down from stage z+1 to stage z. The stages z=1 and z=Z refer, respectively, to the column bottom and top. The total number of stages Z is a model parameter.

By considering that n, T, and P represent the molar flow, temperature, and pressure of each stream, and x_i is the molar fraction of component i (MEA, CO_2, H_2O, N_2, and O_2), the mathematical model can be presented as follow.

B.1 Absorption column mathematical model

B1.1 Overall mass balance in stage z

$$n_{3,z-1} + n_{6,z+1} - n_{3,z} - n_{6,z} = 0 \qquad \text{(B1)}$$

B.1.2 Mass balance for component i in stage z

$$n_{3,z-1} \cdot x_{3,i,z-1} + n_{6,z+1} \cdot x_{6,i,z+1} - n_{3,z} \cdot x_{3,i,z} - n_{6,z} \cdot x_{6,i,z} = 0, \quad i = MEA, CO_2, H_2O, N_2, O_2 \qquad \text{(B2)}$$

$$\sum_i x_{s,z,i} = 1, \quad s = 3,6; \quad i = MEA, CO_2, H_2O, N_2, O_2 \tag{B3}$$

723 B.1.3 Ionic charge relationships in stage z (liquid phase)

$$\begin{aligned} &X_{6,MEAH^+,z} + X_{6,H_3O^+,z} = \\ &X_{6,MEACOO^-,z} + X_{6,HCO_3^-,z} + 2X_{6,CO_3^{2-},z} + X_{6,OH^-,z} \end{aligned} \tag{B4}$$

$$x_{6,MEA,z} = X_{6,MEAH^+,z} + X_{6,MEACOO^-,z} + X_{6,MEA,z} \tag{B5}$$

$$x_{6,CO_2,z} = X_{6,HCO_3^-,z} + X_{6,CO_3^{2-},z} + X_{6,CO_2,z} + X_{6,MEACOO^-,z} \tag{B6}$$

724 B.1.4 Energy balance in stage z

$$\begin{aligned} &n_{3,z-1} \cdot h_{3,z-1} - n_{3,z} \cdot h_{3,z} \\ &+ n_{6,z+1} \cdot \left(h_{6,z+1} \cdot x_{6,\mathrm{CO}_2,z+1} + \Delta H_{R,6,z+1} + x_{6,H_2O,z+1} \cdot \Delta H_{V,6,H_2O,z+1} + x_{6,MEA,z+1} \cdot \Delta H_{V,6,MEA,z+1} \right) \\ &- n_{6,z} \cdot \left(h_{6,z} + x_{6,\mathrm{CO}_2,z} \cdot \Delta H_{R,44,z} + x_{6,H_2O,z} \cdot \Delta H_{V,6,H_2O,z} + x_{6,MEA,z} \cdot \Delta H_{V,6,MEA,z} \right) = 0 \end{aligned} \tag{B7}$$

725 where *h* refers to the enthalpy (molar base), and ΔH_R and ΔH_V are the reaction and vaporization
726 heats, respectively. They are calculated in terms of the temperature and the CO_2 loading factor using
727 correlations suggested in [55] and [56]. The corresponding correlations are presented in the
728 Supplementary Material associated with this article.

729

730 B.1.5 Chemical and phase equilibrium relationships

731 Equilibrium constants K_m of reactions r_1-r_5 are calculated by Eqs. (B8) and (B9), with
732 compositions in molar fraction and temperature in Kelvin:

$$K_{m,z} = \prod_j \left(a_{6,j,z} \right)^{\nu_j} = \prod_j \left(X_{6,j,z} \cdot \gamma_{6,j,z} \right)^{\nu_j}, \quad \begin{matrix} m = r1, r2, r3, r4, r5 \\ j = MEA, MEAH^+, MEACOO^-, \\ CO_2, HCO_3^-, CO_3^{2-}, H_3O^+, OH^- \end{matrix} \tag{B8}$$

$$K_{m,z} = exp\left(A + \frac{B}{T_{6,z}} + C \cdot ln\left(T_{6,z}\right) + D \cdot T_{6,z} + E \cdot T_{6,z}^2 \right), \quad m = r1, r2, r3, r4, r5 \tag{B9}$$

733 $a_{i,z}$, $\gamma_{i,z}$, and ν_i, are, respectively, activity, activity coefficient, and stoichiometric coefficient for
734 component i in reaction m at stage z. As ideal gas behavior is assumed for the liquid phase, the
735 activity coefficients are set to one (Kent-Eisenberg model). The coefficients used in Eq. (B9) are
736 given by [57] and [58], which are provided in the Supplementary Material.

737 The equilibrium phase relationships for reaction r1 and r2-r3 are estimated, respectively, by
738 Eqs. (B10) and (B11):

$$x_{3,i,z} \cdot \varphi_{3,i,z} \cdot P_{3,z} = H_{6,i,z} \cdot \frac{x_{6,i,z}}{\rho_{6,z}}, \quad i = CO_2 \tag{B10}$$

$$x_{3,i,z} \cdot \varphi_{3,i,z} \cdot P_{3,z} = p_{6,i,z} \cdot x_{6,i,z}, \quad i = MEA, H_2O \tag{B11}$$

739 where ρ is the molar density (kmol m^{-3}), *P* the total pressure (kPa), φ the fugacity coefficient in the
740 gas phase (dimensionless), *x* the composition of gas and liquid streams (molar fraction), *H* the
741 Henry's law constant (kPa m^3 $kmol^{-1}$), and *P* the vapor pressure (kPa).
742
743 B.1.6 Stream properties
744 The solubility of CO_2 in MEA solution $H_{6,CO2}$ corrected for solution ionic strength *I* is
745 calculated by Eqs. (B12) to (B14) which are taken from [58] and [59].
746

$$H_{6,CO_2,z} = 10^{0.152\, I_z} \left(x_{6,H_2O,z} \cdot H_{6,CO_2-MEA,z} + x_{6,CO_2,z} \cdot H_{6,CO_2-H_2O,z} \right) \tag{B12}$$

$$H_{6,CO_2-i,z} = \frac{10^{-3}}{\rho_{6,z}} \cdot exp\left(A + \frac{B}{T_{6,z}} + C \cdot ln\left(T_{6,z}\right) + D \cdot T_{6,z} + E \cdot T_{6,z}^2 \right), \quad i = MEA, H_2O \tag{B13}$$

$$I_z = 0.5 \frac{\sum_j \psi_j \cdot X_{6,j,z}}{\rho_{6,z}}, \quad j = MEAH^+, MEACOO^-, H_3O^+, OH^-, HCO_3^-, CO_3^{-2} \tag{B14}$$

747 where ψ_j is the ion charge.
748 Vapor pressure (kPa) is calculated by the Antoine expression:

$$p_{6,i,z} = exp\left(A_i + \frac{B_i}{T_{6,z}} + C_i \cdot ln\left(T_{6,z}\right) + D_i \cdot T_{6,z} + E_i \cdot T_{6,z}^2 \right), \quad i = MEA, H_2O \tag{B15}$$

749 The corresponding coefficients and the coefficients used in Eq. (B13) and (B15) are provided in the
750 Supplementary Material.
751 The calculation of the gas and liquid viscosities are based on a logarithmic form of the mixing
752 rule as suggested in [59]. The solvent viscosity is corrected for the CO_2 presence as in [60].
753 The gas diffusivity is calculated by a modified version of the Chapman-Enskog correlation
754 [61] (Eq. B16). The estimation of CO_2 diffusivity in MEA solution (Eq. B17) is based on the N_2O

analogy [62] which corrects the effect of the CO_2−MEA reaction. The expression is adapted from [63] and [64].

$$D_{3,z} = \sum_i x_{3,i,z} \frac{a_i \cdot T_{3,z}^{1.75}}{P_{3,z}}, \quad i = MEA, CO_2, H_2O, N_2, O_2 \tag{B16}$$

$$D_{6,z} = \left(2.35 \times 10^{-6} e^{-2119 \cdot T_{6,z}^{-1}}\right) \cdot \left(\frac{\mu_{6,H_2O,z}}{\mu_{6,z}}\right)^{0.51} \tag{B17}$$

Correlations taken from [59] are used to compute the enthalpies in the gas and liquid phases (see Supplementary Material).

B.1.6.1 Fugacity coefficient and compressibility factor

The gas-phase fugacity coefficient φ and the compressibility factor fc of a component k are estimated by using the Peng-Robinson equation of state for multi-component systems [65] by Eqs. (B18) and (B19), respectively.

$$\begin{aligned} &\ln\left(\varphi_{k,z}\right) = \frac{b_{PR,k}}{b_{PR,3,z}}\left(fc_{3,z} - 1\right) - \ln\left(fc_{3,z} - B_{PR,3,z}\right) \\ &- \frac{1}{2\sqrt{2}} \cdot \frac{A_{PR,3,z}}{B_{PR,3,z}} \cdot \left(\frac{2\sum_i (x_{3,i,z} \cdot a_{PR,i,k,z})}{a_{PR,3,z}} - \frac{b_{PR,k}}{b_{PR,3,z}}\right) \qquad i \neq k;\ i = MEA, CO_2, H_2O, N_2, O_2 \\ &\ln\left(\frac{fc_{3,z} - 2.414 \cdot B_{PR,3,z}}{fc_{3,z} - 0.414 \cdot B_{PR,3,z}}\right) \end{aligned} \tag{B18}$$

$$\begin{aligned} &fc_{3,z}^3 - fc_{3,z}^2 \cdot \left(1 - B_{PR,3,z}\right) + fc_{3,z}^3 \cdot \left(A_{PR,3,z} - 3 \cdot B_{PR,3,z}^2 - 2 \cdot B_{PR,3,z}\right) + \\ &-\left(A_{PR,3,z} \cdot B_{PR,3,z} - B_{PR,3,z}^2 - B_{PR,3,z}^3\right) = 0 \end{aligned} \tag{B19}$$

The mixture values A and B are calculated by the mixing rules by Eqs. (B20)−(B27):

$$A_{PR,3,z} = \frac{a_{PR,3,z} \cdot P_{3,z}}{R^2 \cdot T_{3,z}^2} \tag{B20}$$

$$a_{PR,3,z} = \sum_i \sum_k (x_{3,i,z} \cdot x_{3,k,z} \cdot a_{PR,i,k}), \quad i \neq k,\ i = MEA, CO_2, H_2O, N_2, O_2 \tag{B21}$$

$$a_{PR,i,k,z} = a_{PR,i,z}^{1/2} \cdot a_{PR,k,z}^{1/2} \cdot \left(1 - \delta_{PR,i,k}\right), \quad i \neq k,\ i = MEA, CO_2, H_2O, N_2, O_2 \tag{B22}$$

$$a_{PR,i,z} = \left(0.45724 \cdot \frac{R^2 \cdot T_{c,i}^2}{P_{c,i}}\right) \cdot \left(1 + \left(1 - \kappa_{PR,i} \cdot \left(\frac{T_{3,z}}{T_{c,i}}\right)^{1/2}\right)\right)^2, \quad i = MEA, CO_2, H_2O, N_2, O_2 \tag{B23}$$

$$\kappa_{PR,i} = 0.37464 + 1.54226 \cdot \omega_{PR,i} - 0.26992 \cdot \omega_{PR,i}^2, \quad i = MEA, CO_2, H_2O, N_2, O_2 \tag{B24}$$

$$B_{PR,3,z} = \frac{b_{PR,3,z} \cdot P_{3,z}}{R \cdot T_{3,z}} \tag{B25}$$

$$b_{PR,3,z} = \sum_i \sum_i (x_{3,i,z} \cdot b_{PR,i}), \quad i = MEA, CO_2, H_2O, N_2, O_2 \tag{B26}$$

$$b_{PR,i} = 0.07780 \cdot \frac{R \cdot Tc_i}{Pc_i}, \quad i = MEA, CO_2, H_2O, N_2, O_2 \tag{B27}$$

where T_c and P_c are the critical temperature and pressure, ω_{PR} the acentric factor, and δ_{PR} a binary interaction coefficient (see Supplementary Material).

B.1.7. Design of the absorption column

B.1.7.1. Column diameter

The diameter of each stage $D_{ABS,z}$ is calculated by:

$$D_{ABS,z} = \left(\frac{4 \cdot n_{3,z}}{\pi \cdot f_{\mathrm{ABS},z} \cdot u_{f,ABS,z} \cdot \rho_{3,z}}\right)^{0.5} \tag{B28}$$

where u_f is the flooding velocity (m s^{-1}) and f is the flooding factor (dimensionless) which ranges from 0.6 to 0.85. The flooding velocity for random packing is calculated according to [66] by Eqs. (B29)–(B31).

$$\Upsilon_z = f_{2,z} \cdot f_{3,z} \cdot \left(\frac{F_p \cdot \left(u_{f\,3,z}\right)^2}{g}\right) \cdot \left(\frac{\rho_{3,z} \cdot MW_{3,z}}{999.53}\right) \tag{B29}$$

$$\Upsilon_z = \exp\left(-3.7121 - 1.0371 \cdot \ln\left(f_{1,z}\right) - 0.1501 \cdot \left(\ln\left(f_{1,z}\right)\right)^2 - 0.00754 \cdot \left(\ln\left(f_{1,z}\right)\right)^3\right) \tag{B30}$$

$$0.01 \le \Upsilon_z \le 10 \tag{B31}$$

where f_1, f_2, and f_3 are dimensionless factors and are provided in the Supplementary Material.

According to [47] and [67], the column diameter expressed in meter should be restricted to:

$$10\, d_p \le D_{ABS,z} \le 12.8 \tag{B32}$$

where d_p is the nominal diameter of packing (model parameter).

B.1.7.2 Column height

The height of the absorption column H_{ABS} depends on the separation requirements and the packing efficiency. The classical NTU−HTU approach is used to compute the stage height $h_{ABS,z}$:

$$H_{ABS} = \sum_{z=1}^{Z} h_{ABS,z} \tag{B33}$$

$$h_{ABS,z} = HTU_z \cdot NTU_z \tag{B34}$$

$$HTU_z = \left(\frac{n_{3,z}}{A_{ABS,z} \cdot R \cdot T_{3,z} \cdot \mathrm{a}_{e,z} \cdot k_{3,z} \cdot \rho_{3,z}} \right) + \Gamma_z \left(\frac{n_{6,z}}{A_{ABS,z} \cdot k_{6,z} \cdot \mathrm{a}_{e,z} \cdot \rho_{6,z} \cdot E_z} \right) \tag{B35}$$

$$NTU_z = -\ln\left(1-\eta_z\right) \tag{B36}$$

$$\eta_z = \frac{x_{3,CO_2,z} - x_{3,CO_2,z-1}}{x^*_{3,CO_2,z} - x_{3,CO_2,z-1}} \tag{B37}$$

$$\Gamma_z = m_{6,z} \cdot \frac{n_{3,z}}{n_{6,z}} \tag{B38}$$

where $a_{e,z}$ is the effective interfacial area for mass transfer ($m^2\ m^{-3}$); Γ the stripping factor; m the slope of the equilibrium line; k_3 (kmol $kPa^{-1}\ s^{-1}\ m^{-2}$) and k_6 ($m\ s^{-1}$) the gas-side and liquid-side mass transfer coefficients, respectively; E the enhancement factor (dimensionless); η the Murphree efficiency (dimensionless); R the universal gas constant (kPa m^3 $kmol^{-1}$ K^{-1}). The superscript * refers to the equilibrium conditions.

The effective *interfacial area* for mass transfer a_e is calculated by the correlation proposed by [68] which is expressed in Eq. (B39):

$$\frac{\mathrm{a}_{e,z}}{a_t} = 1 - \exp\left[-1.45 \left(\frac{\sigma_c}{\sigma_{6,z}} \right)^{0.75} \mathrm{Re}_z^{0.1} \cdot Fr_z^{-0.05} \cdot We_z^{0.2} \right] \tag{B39}$$

where Re, Fr, and We are the Reynolds, Froude, and Weber numbers, respectively; σ_c and a_t refer to the surface tension (N m^{-1}) and total surface area (m^2 m^{-3}) of the packing material (model parameters), respectively; σ_6 is the liquid surface tension (N/m^{-1}).

The influence of reactions r6 and r7 on the CO_2 mass transfer is considered by the enhancement factor E:

$$E_z = \frac{\left[D_{6,CO_2,z} \left(k_{r6,z} \cdot x_{6,\mathrm{MEA},z} + k_{r7,z} \cdot x_{6,CO_2\mathrm{A},z} \right) \right]^{1/2}}{k_{6,z}} \quad \text{(B40)}$$

where D is the diffusivity (m^2/s). The forward constants k_{r6} and k_{r7} of the parallel and kinetically controlled reactions are taken from [69] and [57] and are provided in the Supplementary Material.

A.1.7.3. Column pressure drop

The total pressure drop ΔP_{ABS} (kPa) in the absorption column is calculated by Eq. (B41):

$$\Delta P_{ABS} = \sum_z \Delta P_{ABS,z} \cdot h_{ABS,z} \quad \text{(B41)}$$

where the pressure drop per unit of packing ΔP_z (kPa/m) is estimated by correlations given in [70], which consider the pressure drop associated to the dry packing and to the liquid presence (Eqs. B42−B46):

$$\Delta P_{ABS,z} = 0.8160 \cdot \left(f_{4,z} + 0.4 \cdot f_{4,z}^4 \left(\frac{f_{5,z}}{20000} \right)^{0.1} \right) \quad \text{(B42)}$$

$$f_{4,z} = 7.4 \times 10^{-8} \cdot \left(f_{6,z}^2 \cdot 10^{2.7 \times 10^{-5}} \right) \quad \text{(B43)}$$

$$f_{5,z} = \left(737.38 \frac{n_{6,z} \cdot MW_{6,z}}{A_z} \right) \cdot \left(\frac{999.53}{\rho_{6,z} \cdot MW_{6,z}} \right) \cdot \left(\frac{Fp_d}{64.056} \right)^{0.5} \cdot \left(\frac{\mu_{6,z}}{1000} \right)^{0.2}, \; Fp_d > 61 m^2/m^3 \quad \text{(B44)}$$

$$f_{5,z} = \left(737.38 \cdot \frac{n_{6,z} \cdot MW_{6,z}}{A_z} \right) \cdot \left(\frac{999.53}{\rho_{6,z} \cdot MW_{6,z}} \right) \cdot \left(\frac{64.056}{Fp_d} \right)^{0.5} \cdot \left(\frac{\mu_{6,z}}{1000} \right)^{0.1}, \; Fp_d \leq 61\, m^2/m^3 \quad \text{(B45)}$$

$$f_{6,z} = \left(0.8197 \cdot \frac{n_{3,z} \cdot MW_{3,z}^{0.5}}{A_z \cdot \rho_{3,z}^{0.5}} \right) \cdot \left(\frac{Fp_d}{64.056} \right)^{0.5} \left(10^{0.019 \rho_{3,z} \cdot MW_{3,z}} \right) \quad \text{(B46)}$$

The following constraints impose minimum and maximum permissible column pressure drops per unit of packing height to ensure a minimum vapor flow rate for avoiding laminar vapor flow and having a good vapor distribution [59,71]:

$$0.08\,kPa/m \le \Delta P_{ABS,z} \le 1\,kPa/m \tag{B47}$$

B.2 CO_2 capture level

The percentage of the CO_2 captured in the absorber ($R_{CO2,ABS}$) and the total percentage (R_{CO2}) are calculated by Eqs. (B48) and (B49), respectively:

$$R_{CO_2,ABS} = 100\ \frac{n_2 x_{CO_2,2} - n_4 x_{CO_2,4}}{n_2 x_{CO_2,2}} \tag{B48}$$

$$R_{CO_2} = 100\ \frac{n_{26} x_{CO_2,26}}{n_2 x_{CO_2,2}} \tag{B49}$$

References

[1] R.M. Cuéllar-Franca, A. Azapagic, Carbon capture, storage and utilisation technologies: A critical analysis and comparison of their life cycle environmental impacts, J. CO2 Util. 9 (2015) 82–102. doi:10.1016/j.jcou.2014.12.001.

[2] Z. Kravanja, P.S. Varbanov, J.J. Klemeš, Recent advances in green energy and product productions, environmentally friendly, healthier and safer technologies and processes, CO2 capturing, storage and recycling, and sustainability assessment in decision-making, Clean Technol. Environ. Policy. 17 (2015) 1119–1126. doi:10.1007/s10098-015-0995-9.

[3] A. Chikukwa, N. Enaasen, H.M. Kvamsdal, M. Hillestad, Dynamic Modeling of Post-combustion CO2 Capture Using Amines–A Review, Energy Procedia. 23 (2012) 82–91. doi:10.1016/j.egypro.2012.06.063.

[4] L.E. Øi, S.H.P. Kvam, Comparison of Energy Consumption for Different CO2 Absorption Configurations Using Different Simulation Tools, Energy Procedia. 63 (2014) 1186–1195. doi:10.1016/j.egypro.2014.11.128.

[5] J.C. Glier, E.S. Rubin, Assessment of solid sorbents as a competitive post-combustion CO2 capture technology, Energy Procedia. 37 (2013) 65–72. doi:10.1016/j.egypro.2013.05.086.

[6] W. Zhang, J. Chen, X. Luo, M. Wang, Modelling and process analysis of post-combustion carbon capture with the blend of 2-amino-2-methyl-1-propanol and piperazine, Int. J. Greenh. Gas Control. 63 (2017) 37–46. doi:10.1016/j.ijggc.2017.04.018.

[7] A.A. Hinai, M.A. Zahra, Study of Novel Solvents and 2MAE Blends for CO2 Post-Combustion Capture, Energy Procedia. 114 (2017) 686–692. doi:10.1016/j.egypro.2017.03.1211.

[8] J. Narku-Tetteh, P. Muchan, C. Saiwan, T. Supap, R. Idem, Selection of components for formulation of amine blends for post-combustion CO2 capture based on the side chain structure of primary, secondary and tertiary amines, Chem. Eng. Sci. 170 (2017) 542–560. doi:10.1016/j.ces.2017.02.036.

[9] J. Burger, V. Papaioannou, S. Gopinath, G. Jackson, A. Galindo, C.S. Adjiman, A hierarchical method to integrated solvent and process design of physical CO2 absorption using the SAFT-γ Mie approach, AIChE J. 61 (2015) 3249–3269. doi:10.1002/aic.14838.

[10] F.K. Chong, V. Andiappan, D.K.S. Ng, D.C.Y. Foo, F.T. Eljack, M. Atilhan, N.G. Chemmangattuvalappil, Design of Ionic Liquid as Carbon Capture Solvent for a Bioenergy System: Integration of Bioenergy and Carbon Capture Systems, ACS Sustain. Chem. Eng. 5 (2017) 5241–5252. doi:10.1021/acssuschemeng.7b00589.
[11] A.I. Papadopoulos, S. Badr, A. Chremos, E. Forte, T. Zarogiannis, P. Seferlis, S. Papadokonstantakis, C.S. Adjiman, A. Galindo, G. Jackson, Efficient screening and selection of post-combustion CO2 capture solvents, Chem. Eng. Trans. 39 (2014) 211–216. doi:10.3303/CET1439036.
[12] F. Porcheron, A. Gibert, P. Mougin, A. Wender, High Throughput Screening of CO2 Solubility in Aqueous Monoamine Solutions, Environ. Sci. Technol. 45 (2011) 2486–2492. doi:10.1021/es103453f.
[13] M. Stavrou, M. Lampe, A. Bardow, J. Gross, Continuous Molecular Targeting–Computer-Aided Molecular Design (CoMT–CAMD) for Simultaneous Process and Solvent Design for CO2 Capture, Ind. Eng. Chem. Res. 53 (2014) 18029–18041. doi:10.1021/ie502924h.
[14] V. Venkatraman, M. Gupta, M. Foscato, H.F. Svendsen, V.R. Jensen, B.K. Alsberg, Computer-aided molecular design of imidazole-based absorbents for CO2 capture, Int. J. Greenh. Gas Control. 49 (2016) 55–63. doi:10.1016/j.ijggc.2016.02.023.
[15] X. Li, S. Wang, C. Chen, Experimental Study of Energy Requirement of CO2 Desorption from Rich Solvent, Energy Procedia. 37 (2013) 1836–1843. doi:10.1016/j.egypro.2013.06.063.
[16] M. Rabensteiner, G. Kinger, M. Koller, G. Gronald, C. Hochenauer, Investigation of carbon dioxide capture with aqueous piperazine on a post-combustion pilot plant–Part I: Energetic review of the process, Int. J. Greenh. Gas Control. 39 (2015) 79–90. doi:10.1016/j.ijggc.2015.05.003.
[17] M. Leimbrink, S. Tlatlik, S. Salmon, A.-K. Kunze, T. Limberg, R. Spitzer, A. Gottschalk, A. Górak, M. Skiborowski, Pilot scale testing and modeling of enzymatic reactive absorption in packed columns for CO2 capture, Int. J. Greenh. Gas Control. 62 (2017) 100–112. doi:10.1016/j.ijggc.2017.04.010.
[18] S.A. Freeman, J. Davis, G.T. Rochelle, Degradation of aqueous piperazine in carbon dioxide capture, Int. J. Greenh. Gas Control. 4 (2010) 756–761. doi:10.1016/j.ijggc.2010.03.009.
[19] Y. Du, Y. Wang, G.T. Rochelle, Thermal degradation of novel piperazine-based amine blends for CO2 capture, Int. J. Greenh. Gas Control. 49 (2016) 239–249. doi:10.1016/j.ijggc.2016.03.010.
[20] V. Cuzuel, C. Gouedard, L. Cuccia, J. Brunet, A. Rey, J. Dugay, J. Vial, F. Perbost-Prigent, J. Ponthus, V. Pichon, P.-L. Carrette, Amine degradation in CO2 capture. 4. Development of complementary analytical strategies for a comprehensive identification of degradation compounds of MEA, Int. J. Greenh. Gas Control. 42 (2015) 439–453. doi:10.1016/j.ijggc.2015.08.022.
[21] A. Alshehri, R. Khalilpour, A. Abbas, Z. Lai, Membrane Systems Engineering for Post-combustion Carbon Capture, Energy Procedia. 37 (2013) 976–985. doi:10.1016/j.egypro.2013.05.193.
[22] A.M. Arias, M.C. Mussati, P.L. Mores, N.J. Scenna, J.A. Caballero, S.F. Mussati, Optimization of multi-stage membrane systems for CO2 capture from flue gas, Int. J. Greenh. Gas Control. 53 (2016) 371–390. doi:10.1016/j.ijggc.2016.08.005.
[23] B. Belaissaoui, D. Willson, E. Favre, Membrane gas separations and post-combustion carbon dioxide capture: Parametric sensitivity and process integration strategies, Chem. Eng. J. 211 (2012) 122–132. doi:10.1016/j.cej.2012.09.012.
[24] X. He, C. Fu, M.-B. Hägg, Membrane system design and process feasibility analysis for CO2 capture from flue gas with a fixed-site-carrier membrane, Chem. Eng. J. 268 (2015) 1–9. doi:10.1016/j.cej.2014.12.105.

[25] N.C. Mat, G.G. Lipscomb, Membrane process optimization for carbon capture, Int. J. Greenh. Gas Control. 62 (2017) 1–12. doi:10.1016/j.ijggc.2017.04.002.
[26] T.C. Merkel, H. Lin, X. Wei, R. Baker, Power plant post-combustion carbon dioxide capture: An opportunity for membranes, J. Membr. Sci. 359 (2010) 126–139. doi:10.1016/j.memsci.2009.10.041.
[27] S. Roussanaly, R. Anantharaman, K. Lindqvist, H. Zhai, E. Rubin, Membrane properties required for post-combustion CO2 capture at coal-fired power plants, J. Membr. Sci. 511 (2016) 250–264. doi:10.1016/j.memsci.2016.03.035.
[28] C.A. Scholes, M.T. Ho, A.A. Aguiar, D.E. Wiley, G.W. Stevens, S.E. Kentish, Membrane gas separation processes for CO2 capture from cement kiln flue gas, Int. J. Greenh. Gas Control. 24 (2014) 78–86. doi:10.1016/j.ijggc.2014.02.020.
[29] H. Zhai, E.S. Rubin, Techno-economic assessment of polymer membrane systems for postcombustion carbon capture at coal-fired power plants, Environ. Sci. Technol. 47 (2013) 3006–3014. doi:10.1021/es3050604.
[30] K. Lindqvist, S. Roussanaly, R. Anantharaman, Multi-stage Membrane Processes for CO2 Capture from Cement Industry, Energy Procedia. 63 (2014) 6476–6483. doi:10.1016/j.egypro.2014.11.683.
[31] P.L. Mores, J.I. Manassaldi, N.J. Scenna, J.A. Caballero, M.C. Mussati, S.F. Mussati, Optimization of the design, operating conditions, and coupling configuration of combined cycle power plants and CO2 capture processes by minimizing the mitigation cost, Chem. Eng. J. 331 (2018) 870–894. doi:10.1016/j.cej.2017.08.111.
[32] X. He, D.R. Nieto, A. Lindbråthen, M.-B. Hägg, Membrane System Design for CO2 Capture, in: A.I. Papadopoulos, P. Seferlis (Eds.), Process Syst. Mater. CO2 Capture, John Wiley & Sons, Ltd, 2017: pp. 249–281. http://dx.doi.org/10.1002/9781119106418.ch10.
[33] E. Favre, Membrane processes and postcombustion carbon dioxide capture: Challenges and prospects, Chem. Eng. J. 171 (2011) 782–793. doi:10.1016/j.cej.2011.01.010.
[34] B. Freeman, Y. Yampolskii, Membrane Gas Separation, Wiley, 2011.
[35] R. Bounaceur, N. Lape, D. Roizard, C. Vallieres, E. Favre, Membrane processes for post-combustion carbon dioxide capture: A parametric study, Energy. 31 (2006) 2556–2570. doi:10.1016/j.energy.2005.10.038.
[36] P. Mores, N. Scenna, S. Mussati, CO2 capture using monoethanolamine (MEA) aqueous solution: Modeling and optimization of the solvent regeneration and CO2 desorption process, Energy. 45 (2012) 1042–1058. doi:10.1016/j.energy.2012.06.038.
[37] P. Mores, N. Scenna, S. Mussati, A rate based model of a packed column for CO2 absorption using aqueous monoethanolamine solution, Int. J. Greenh. Gas Control. 6 (2012) 21–36. doi:10.1016/j.ijggc.2011.10.012.
[38] P. Mores, N. Scenna, S. Mussati, Post-combustion CO2 capture process: Equilibrium stage mathematical model of the chemical absorption of CO2 into monoethanolamine (MEA) aqueous solution, Chem. Eng. Res. Des. 89 (2011) 1587–1599. doi:10.1016/j.cherd.2010.10.012.
[39] A.M. Arias, P.L. Mores, N.J. Scenna, S.F. Mussati, Optimal design and sensitivity analysis of post-combustion CO2 capture process by chemical absorption with amines, J. Clean. Prod. 115 (2016) 315–331. doi:10.1016/j.jclepro.2015.12.056.
[40] P. Feron, Absorption-Based Post-Combustion Capture of Carbon Dioxide, Elsevier Science, 2016.
[41] A. González-Díaz, A.M. Alcaráz-Calderón, M.O. González-Díaz, Á. Méndez-Aranda, M. Lucquiaud, J.M. González-Santaló, Effect of the ambient conditions on gas turbine combined cycle power plants with post-combustion CO2 capture, Energy. 134 (2017) 221–233. doi:10.1016/j.energy.2017.05.020.

[42] G.T. Rochelle, Amine Scrubbing for CO2 Capture, Science. 325 (2009) 1652–1654. doi:10.1126/science.1176731.
[43] L.E. Øi, J. Lundberg, M. Pedersen, P.M. Hansen, M.C. Melaaen, Laboratory Rig for Atmospheric CO2 Absorption and Desorption under Pressure, Energy Procedia. 37 (2013) 1933–1940. doi:10.1016/j.egypro.2013.06.074.
[44] M.R.M. Abu-Zahra, J.P.M. Niederer, P.H.M. Feron, G.F. Versteeg, CO2 capture from power plants: Part II. A parametric study of the economical performance based on mono-ethanolamine, Int. J. Greenh. Gas Control. 1 (2007) 135–142. doi:10.1016/S1750-5836(07)00032-1.
[45] A.B. Rao, E.S. Rubin, A Technical, Economic, and Environmental Assessment of Amine-Based CO2 Capture Technology for Power Plant Greenhouse Gas Control, Environ. Sci. Technol. 36 (2002) 4467–4475. doi:10.1021/es0158861.
[46] Mayer, E, Chemical Engineering Plant Cost CEPCI 2014, 2016.
[47] W.D. Seider, J.D. Seader, D.R. Lewin, S. Widagdo, Product and Process Design Principles: Synthesis, Analysis and Design, 3 edition, John Wiley & Sons, Hoboken, NJ, 2008.
[48] McCollum, David L., Ogden, Joan M., Techno-economic models for carbon dioxide compression, transport, and storage & correlations for estimating carbon dioxide density and viscosity., Institute of Transportation Studies, University of California, Davis, California, Davis, USA, 2006.
[49] Fisher, Kevin S., Beitler, Carrie, Rueter, Curtis, Searcy, Katherine, Rochelle, Gary, Jassim, Majeed, Figueroa, José D., Integrating MEA regeneration with CO2 compression to reduce CO2 capture costs, in: Conf. Proc., Alexandria Virginia, USA, 2005.
[50] Ulrich, Gael D., Vasudevan, Palligarnai T., How to Estimate Utility Costs, (2006). http://www.chemengonline.com/how-to-estimate-utility-costs/?printmode=1 (accessed February 26, 2018).
[51] Henao Uribe, Carlos Andrés, Simulación y evaluación de procesos químicos, Universidad Pontificia Bolivariana, 2005.
[52] GAMS Development Corporation, General Algebraic Modeling System (GAMS) Release 23.6.5, Washington, DC, USA, 2010. http://www.gams.com/.
[53] A. Drud, CONOPT 3 solver manual, ARKI Consulting and Development A/S, Bagsvaerd, Denmark, 2012.
[54] S. Roussanaly, R. Anantharaman, Cost-optimal CO2 capture ratio for membrane-based capture from different CO2 sources, Chem. Eng. J. 327 (2017) 618–628. doi:10.1016/j.cej.2017.06.082.
[55] B.A. Oyenekan, G.T. Rochelle, Rate modeling of CO2 stripping from potassium carbonate promoted by piperazine, Int. J. Greenh. Gas Control. 3 (2009) 121–132. doi:10.1016/j.ijggc.2008.06.010.
[56] M.D. Hilliard, A predictive thermodynamic model for an aqueous blend of potassium carbonate, piperazine, and monoethanolamine for carbon dioxide capture from flue gas, Ph.D. Dissertation, The University of Texas at Austin, 2008. https://repositories.lib.utexas.edu/handle/2152/3900 (accessed June 28, 2018).
[57] A. Aboudheir, P. Tontiwachwuthikul, A. Chakma, R. Idem, Kinetics of the reactive absorption of carbon dioxide in high CO2-loaded, concentrated aqueous monoethanolamine solutions, Chem. Eng. Sci. 58 (2003) 5195–5210. doi:10.1016/j.ces.2003.08.014.
[58] Y. Liu, L. Zhang, S. Watanasiri, Representing Vapor−Liquid Equilibrium for an Aqueous MEA−CO2 System Using the Electrolyte Nonrandom-Two-Liquid Model, Ind. Eng. Chem. Res. 38 (1999) 2080–2090. doi:10.1021/ie980600v.
[59] T. Greer, Modeling and simulation of post-combustion CO2 capturing, M.Sc. thesis, Telemark University College, Faculty of Technology, 2008. https://brage.bibsys.no/xmlui/handle/11250/2439027 (accessed June 28, 2018).

[60] D.-K Hansen, Dynamic modeling of an absorption tower for the removal of carbon dioxide from exhaust gas by means of Monoethanolamine, M.Sc. thesis, Telemark University College, Faculty of Technology., 2004.
[61] R.C. Reid, J.M. Prausnitz, B.E. Poling, The properties of gases and liquids, McGraw-Hill, New York, 1987.
[62] H.A. Al-Ghawas, D.P. Hagewiesche, G. Ruiz-Ibanez, O.C. Sandall, Physicochemical properties important for carbon dioxide absorption in aqueous methyldiethanolamine, J. Chem. Eng. Data. 34 (1989) 385–391. doi:10.1021/je00058a004.
[63] G.F. Versteeg, W.P.M. Van Swaaij, Solubility and diffusivity of acid gases (carbon dioxide, nitrous oxide) in aqueous alkanolamine solutions, J. Chem. Eng. Data. 33 (1988) 29–34. doi:10.1021/je00051a011.
[64] R. Maceiras, E. Álvarez, M.Á. Cancela, Effect of temperature on carbon dioxide absorption in monoethanolamine solutions, Chem. Eng. J. 138 (2008) 295–300. doi:10.1016/j.cej.2007.05.049.
[65] D.-Y. Peng, D.B. Robinson, A New Two-Constant Equation of State, Ind. Eng. Chem. Fundam. 15 (1976) 59–64. doi:10.1021/i160057a011.
[66] M. Leva, Reconsider packed-tower pressure-drop correlations, Chem Eng ProgChemical Eng. Prog. N. Y. 88 (1992) 65–72.
[67] D.G. Chapel, C.L. Mariz, J. Ernest, Recovery of CO2 from Flue Gases: Commercial Trends, in: Can. Soc. Chem. Eng. Annu. Meet., Saskatoon, Saskatchewan, Canada, 1999.
[68] K. Onda, H. Takeuchi, Y. Okumoto, MASS TRANSFER COEFFICIENTS BETWEEN GAS AND LIQUID PHASES IN PACKED COLUMNS, J. Chem. Eng. Jpn. 1 (1968) 56–62. doi:10.1252/jcej.1.56.
[69] L. Kucka, E.Y. Kenig, A. Górak, Kinetics of the Gas−Liquid Reaction between Carbon Dioxide and Hydroxide Ions, Ind. Eng. Chem. Res. 41 (2002) 5952–5957. doi:10.1021/ie020452f.
[70] L.A. Robbins, Improve pressure-drop prediction with a new correlation, Chem. Eng. Prog. 87 (1991) 87–90.
[71] H.Z. Kister, Distillation Design, 1 edition, McGraw-Hill Education, New York, 1992.